journal

J. Am. Ceram. Soc., 95 [4] 1147–1162 (2012)
DOI: 10.1111/j.1551-2916.2012.05099.x

High Speed SPM Applied for Direct Nanoscale Mapping of the Influence of Defects on Ferroelectric Switching Dynamics

Bryan D. Huey,[‡,†] Ramesh Nath Premnath,[‡] Sungjun Lee,[‡,§] and Nicholas A. Polomoff[‡]

[‡]Institute of Materials Science, University of Connecticut, Storrs, Connecticut

[§]Division of Physical Metrology, Korea Research Institute of Standards and Science, Daejeon, Korea

A high speed variation of Scanning Probe Microscopy with continuous image rates on the order of 1 frame per second is applied to investigate the nucleation and growth of individual ferroelectric domains. Movies of consecutive images directly identify nascent domains and their nucleation times, while tracking their development with time and voltage reveals linear domain growth at lateral velocities near 1 mm/s, even faster for nascent domains. Nanoscale maps of nucleation times and growth velocities indicate that domain nucleation and growth are uncorrelated, varying extensively with position. Domain switching dynamics do strongly couple to film defects; for instance, grain boundaries can profoundly pin domain walls, and polarization reversal kinetics are influenced by strain fields near microcracks or in asymmetric specimens. The influence of the onset of switching fatigue is observed as well. These results highlight the importance of updating classical interpretations of ferroelectric switching for truly rigorous models of polarization dynamics. Coupling high speed SPM imaging with *in situ* activation by voltage or other parameters therefore provides an important methodology to research dynamic surface properties with nanoscale resolution, extendable to a range of materials such as photovoltaics, thermoelectrics, batteries, fuel cells, multiferroics, phase change systems, etc.

I. Introduction

Atomic Force Microscopy (AFM) has advanced significantly since its invention in 1986,[1] with a wealth of variations designed to measure and/or manipulate the nanoscale properties of semiconductors, polymers, metals, biological specimens, and of course ceramics.[2] This work employs one such variation for dynamics studies, specifically of the polarization of ferroelectric domains. Generally, imaging speed remains a limitation for dynamics work with AFM-based techniques, except for a few highly customized systems worldwide[3–18] which are primarily applied to biological specimens, for high throughput imaging, or for lithography.[19–29] The High Speed Scanning Property Mapping (HSSPM) approach employed here, on the other hand, is based on a standard AFM as well as common test and measurement hardware, minimizing startup costs.[23,30] This method couples principles of ultrasonics and AFM[31–39] by actuating and monitoring the AFM probe at high frequency contact resonances (>1 MHz), providing property contrast based on amplitude and phase images[32,40–43] with equivalent resolution as standard-speed AFM images.

The HSSPM method leverages a relative insensitivity of contact resonances to variations in applied force, because to achieve such high speed scanning with standard AFM equipment (up to a cm/s) the images are acquired without active feedback.[44] Notably, previously reported high speed property measurements based on free resonant detection required active damping of the oscillating tip and cantilever (otherwise the response at a particular pixel continues to "ring" into adjacent pixels, smearing the image).[20,45] Contact resonances, on the other hand, are essentially passively damped (resonant quality factors are typically less than one tenth of those for free resonant levers), and are therefore inherently amenable to high speed scanning. For smooth surfaces HSSPM can thus be easily configured for high speed mapping of electric, magnetic, mechanical, and/or coupled properties such as piezoactuation.[23]

Ferroelectric thin films are particularly attractive for HSSPM studies, as the method's high throughput and sensitivity to ferroelectric domain orientation make novel nanoscale dynamic studies feasible.[30] Here, HSSPM is applied to directly quantify individual domain nucleation and growth during *in situ* polarization reversal. This is achieved by operating HSSPM in the Piezo Force Microscopy (PFM) mode, whereby a conducting AFM probe is biased with superimposed AC and DC voltages to generate an electric field across the piezoelectric sample beneath the scanning tip (Fig. 1). For typical biases less than 10 Volts, this results in a picometer-scale local strain of the sample surface via converse piezoactuation, which is then transduced by the AFM tip to normal and/or lateral vibrations of the integrated AFM cantilever. Although such signals are weak, they are well within the range of detection for modern hardware such as lock-in amplifiers.

D. J. Green—contributing editor

Manuscript No. 30405. Received September 29, 2011; approved January 13, 2012.
[†]Author to whom correspondence should be addressed. e-mail: bhuey@ims.uconn.edu

Feature

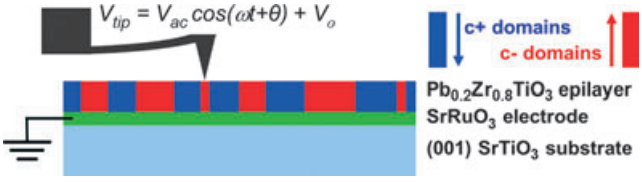

Fig. 1. Schematic of high speed PFM measurement, including $PbZr_{0.2}Ti_{0.8}O_3$ thin film with pure *c* domain structure grown epitaxially on a grounded $SrRuO_3$ electrode and a (001) $SrTiO_3$ substrate.

As an example, Fig. 2 presents standard (1 Hz, left) and high speed (256 Hz, right) PFM images of an epitaxial ferroelectric $PbZrTiO_3$ (PZT) specimen with scale bars as shown. The bottom row displays piezoresponse phase images, with white and black contrast indicating domains oriented into, or out of, the specimen surface. Technically, this contrast signifies a 180° difference in the local piezoactuation beneath the conducting AFM tip when applying an AC field to oppositely poled domains. The top row shows piezoresponse amplitude images, with the signal necessarily nulling at domain walls which are therefore easily identified by dark contrast. Subtle contrast differences between domains oriented in and out of the plane are also frequently apparent in PFM amplitude images due to charging effects, artifacts related to AFM resonances, and/or asymmetric hysteresis loops.

The high speed images, zoomed in to an area of 1.2 μm × 1.2 μm as sketched, were acquired simultaneously in just 1 s, at least 250 times faster than standard PFM imaging. To achieve this, high speed data acquisition is employed to record the piezoresponse amplitude and phase every 15.26 μs, equivalent to 128 pixel per line resolution in each scan direction. Of course more pixels can be acquired for higher resolution images, as long as lock-in amplifiers with shorter time constants can be accessed. Compared with the conventional PFM image of the same region but for a slightly larger area (3 μm × 3 μm), all domain features are clearly resolved with little apparent degradation due to the fast scanning. HSSPM therefore provides the nanoscale property resolution expected of techniques based on scanning

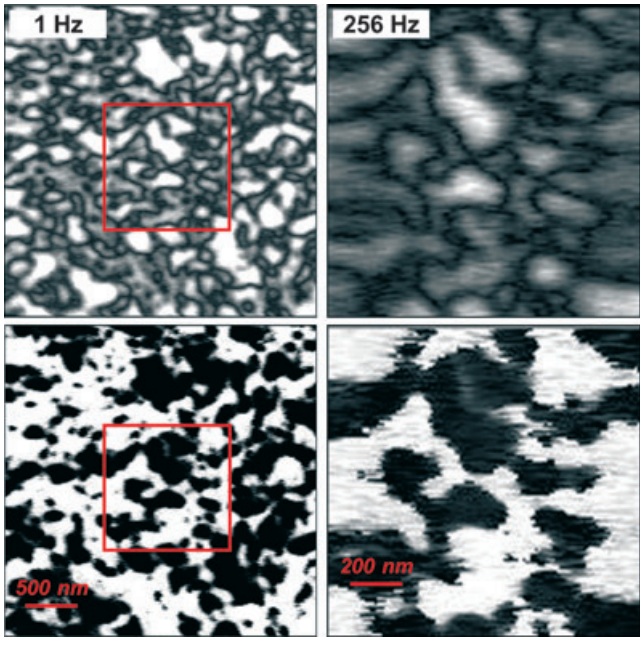

Fig. 2. Standard speed (1 Hz line rate, left) and high speed (256 Hz, right) PFM amplitude (top) and phase (base) images of PZT showing nearly equivalent imaging resolution as fast as 1 frame per second.

probe microscopy, but with a substantially improved imaging rate on the order of full frames per second.

Leveraging this enhancement in efficiency, obvious applications for HSSPM include large area scanning, high throughput (especially manufacturing) settings, and the focus of this work, dynamic property mapping. For ferroelectrics in particular, domains of various orientations, specimens (or regions of specimens) of various compositions, and properties as a function of external stimuli such as temperature or field, all yield distinct piezoresponse amplitudes and/or phases with respect to the actuating voltage. Operating HSSPM in this PFM mode thus provides a powerful means to investigate piezoelectric materials with nanoscale resolution.[46–48]

Of course numerous PFM measurements have been reported previously using standard-speed imaging, requiring anywhere on the order of one frame every 4 min (256 × 256 resolution at 1 Hz line rates) to as long as several hours for complex specimens and image acquisition. Many groups have written prolifically on this topic, with several excellent reviews[49–55] and even books[56–58] devoted to PFM. Published over more than a decade, these works developed the method, improved the understanding of the contrast mechanisms, enhanced equipment and software, and applied PFM to an enormous range of materials and device architectures.

This article specifically focuses on *in situ* switching of ferroelectric domains during rapid scanning of an SPM tip to directly monitor polarization reversal dynamics. Of course many such experiments have already been performed with standard PFM to study domain dynamics,[59–73] some by monitoring domain relaxation over periods as long as hours to days after poling,[74–76] others by serially pulsing and then imaging,[77–82] and others using a dynamic variation of switching spectroscopy PFM.[83–85] Most focused on domain growth and/or relaxation,[30,75,78,80,86–95] with some emphasizing domain nucleation events,[81,96–99] defect structures,[100–104] and even domain structures resolved in three dimensions via serial imaging and cross sections.[105,106] Techniques such as X-ray diffraction[107,108] and TEM[109,110] have provided complementary insight into such switching processes, whereas a wealth of optical investigations with $LiNbO_3$ and related materials have similarly been performed to investigate poling,[111,112] domain walls,[113,114] defects,[115,116] and stress effects.[117] The enhanced imaging speed and high resolution of HSSPM extends such work by providing substantially more data in an experimentally reasonable time, enabling high temporal resolution over longer poling durations, facilitating investigations into more variables, and easing rigorous statistical analyses. Table I summarizes such results presented in the sections that follow, along with their spatial resolution.

Notably, although the results presented herein emphasize ferroelectric domain dynamics, SPM detection of electric and magnetic fields, thermal gradients, optical coupling, etc. is also commonplace. The root concept in HSSPM, i.e., fast AFM-based detection to enable direct nanoscale observation of discrete steps in an evolving process, is therefore feasible for investigating dynamic phenomena for a much wider range of ceramic systems, such as photovoltaics, batteries, fuel cells, phase change materials, thermoelectrics, and the like. The various approaches presented herein to analyze the correspondingly large datasets ("movies"), including area averaging, feature tracking, property histograms, and mapping as a function of time, position, and/or extrinsic variables, are thus broadly applicable especially as high speed SPM capabilities become more widespread.

II. Materials and Methods

The HSSPM measurements have been performed with Asylum Research MFP-3d and Cypher microscopes operated in contact mode, although the high speed concept is platform independent. A repulsive setpoint force on the order of

Table I. Summary of Measurements, Resolution, and Section Discussed

Ferroelectric parameter	Resolution	Section
Domain nucleation	Local (nm)	Direct Observation of Domain Dynamics
Domain growth	Local	
Switching mechanism	Mesoscale (nm sampling of um area)	Aerial Switching
Nucleation time, growth velocity	Both (local and mesoscale)	Individual Domain Nucleation Times and Growth Velocities
Statistical analyses	Mesoscale	
Switching maps	Local	
Fatigue effects	Both	Cycling Studies
Hysteresis loops	Both	Ferroelectric Hysteresis Mapping
Coercive mapping	Mesoscale	
Density of nucleation states	Mesoscale	
Theoretical approaches	Both	A Classic Approach
Line defects (Grain Boundaries, Cracks)	Local	Switching and Defects

500 nN was typically employed, using Nanosensors conductive-diamond-coated cantilevers (~40 nN/nm spring constant). To map the piezoactuation amplitude and phase, an AC bias of up to 5 V peak-to-peak was applied directly to the conducting AFM tip during continuous scanning at line rates from 40 to 256 Hz. Switching was achieved with the simultaneous application of an additional DC bias up to 2.5 V (combined they must exceed the coercive potential for these films, ~3 V). An AC frequency of ~1.6 MHz was applied. Additional hardware included a signal generator (Agilent 33250), lock-in amplifier (SRS844), high speed data acquisition card (Measurement Computing DAS-4020), and external computer control (Agilent Vee).

To directly study individual domain switching by following nucleation and growth during poling with a HSSPM probe, epitaxial PZT thin films have primarily been employed. These epitaxial $PbZr_{0.2}Ti_{0.8}O_3$ (PZT) thin films were prepared by the Ramesh group using pulsed laser deposition as described elsewhere.[118] They exhibit a geometry as sketched in Fig. 1, where a 30–150 nm $Pb_{0.2}Zr_{0.8}TiO_3$ (PZT) epilayer is grown on a vicinal (001) $SrTiO_3$ (STO) substrate with an intermediate (50 nm) $SrRuO_3$ (SRO) epilayer for grounding as a back-electrode during PFM.

Some such specimens exhibit ferroelectric domains oriented purely along the c-axis, normally into, or out of, the sample. Others also include in-plane (100) oriented "a" domains, appearing as a cross-hatched pattern with spacing on the order of 100 nm. To monitor domain dynamics for either specimen type, a sample region is initially poled in the "c+" direction by purely DC-biasing the tip beyond the coercive potential for the film, for instance while scanning a square region with −5 V with respect to the grounded back-electrode. By next repeatedly scanning this area while applying both an oppositely poled DC offset (for switching) as well as a small AC bias (for imaging), domain switching from the initial orientation of *c*+ domains to the opposite *c*- direction is simultaneously activated and imaged.

The superimposed AC + DC potentials are typically selected to be sufficiently small that only the crest of the sinusoidal signal surpasses the coercive field. This practically results in the continuous application of narrow poling pulses that is optimally less than 100 ns wide each (66 ns for an effective 10% duty cycle of a normal 1.5 MHz excitation, repeating once per period so every 666 ns). With an HSSPM line scanning rate of 40 Hz and 256 pixel per line resolution (48.8 μs per pixel for each scan direction), 73 of these nanosecond pulses are thus applied per pixel, amounting to temporal resolution of 4.88 μs of poling, per pixel, per image frame under these conditions.

Naturally such high speed data collection and imaging is challenging, and there are several limitations associated with this approach. For fast imaging, the AFM system and scanner design is crucial, with top speeds dictated by the onset of system mechanical resonances. The maximum practical rate of data collection, on the other hand, depends on the longest time constant of several distinct factors: excitation frequency (a function of cantilever geometry and/or impedance matching), detection rate (AFM detector bandwidth, lock-in-amplifier time constant), and capture rate (data acquisition rate, write time to data storage). Finally, appropriate time constants for the physical phenomena under investigation are obviously crucial as well. Within these constraints, however, the concepts presented throughout this article can be extended to periodic thermal, optical, electric field or magnetic field excitations[119] for similar functional HSSPM studies into nanoscale dynamics with multiferroic systems, optoelectronics, magneto-optics, thermoelectrics, etc.

III. Direct Observation of Domain Dynamics

Focusing initially on nascent domains, Fig. 3 displays 10 pairs of HSSPM amplitude (left) and phase (right) images during poling across a 500 nm × 500 nm region, taken from a "switching movie" of nearly 100 consecutive frames. The phase contrast again identifies domain orientation as with Fig. 2, with dark and light representing a 180° phase shift for c− and c+ domains aligned into and out of the sample, respectively. Dark features in the amplitude contrast indicate the presence of domain walls, again as before. Accordingly, the first few images in Fig. 3 (0 μs) are featureless because the sample is initially uniformly prepoled. This corresponds to "Stage 0" in Fig. 4, which schematically represents a cross section of a nucleating and growing domain along with PFM amplitude and phase signal cross sections. Eventually (after 176 μs of accumulated poling in Fig. 3, sketched as Stage 6 in Fig. 4), the contrast for individual domains behaves as expected, with striking phase contrast for oppositely oriented domains and amplitude images clearly revealing circumferential domain walls defining boundaries between anti-parallel c domains. For intermediate stages of nucleation and growth, however, the contrast variations can only be understood by more carefully considering the ensemble of the entire tip-sample interaction. Although rigorously applicable to all forms of SPM, this is generally only crucial for features smaller than the tip-sample contact area (such as nascent domains), in which case they can be identified but not fully resolved akin to imaging sub-Raleigh-resolution features in optical or transmission electron microscopy.

For example, at t = 59 μs, Stage 2 in Fig. 4, several areas of dark amplitude contrast suggest the presence of such sub-resolution nascent domains (including a domain labeled as "X" in Fig. 3). The phase signal appears to remain unchanged, because of the area-weighted average of the piezoresponse for the very small new domain compared to the larger oppositely poled surrounding region. At t = 78 μs, stage 3, the amplitude at the nucleation site has decreased to

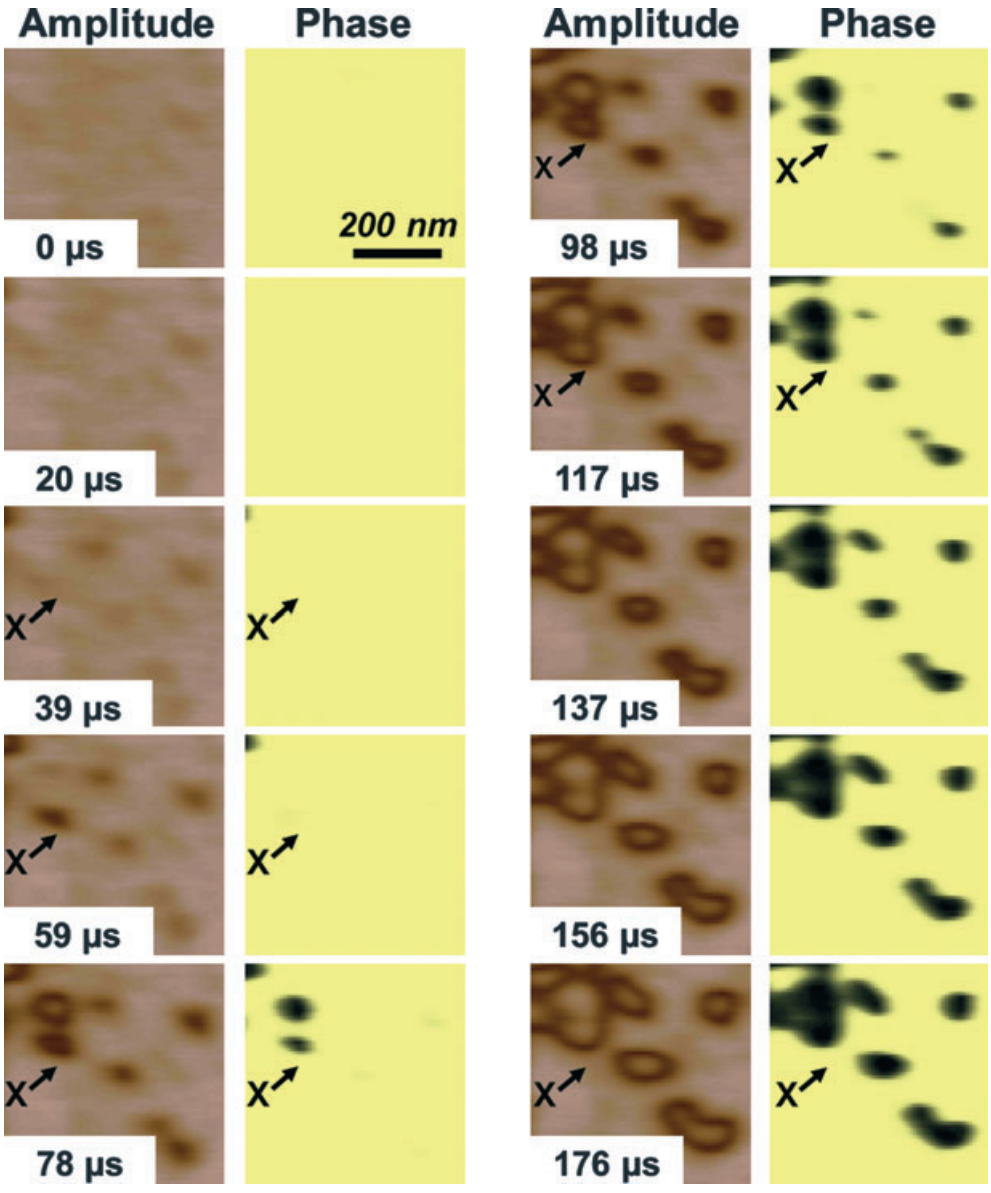

Fig. 3. Evolution of domain switching via nucleation and growth with PFM amplitude and phase images acquired from a 500 nm × 500 nm region (cumulative poling times are indicated for each image pair).

a minimum, while the phase shifts abruptly. At this point the piezoresponse from the new domain now contributes more than half of the signal detected beneath the scanned probe tip, providing an estimate of the tip-sample contact radius (10–15 nm based on Fig. 3). Domain "X" becomes still more apparent at $t = 98$ μs, Stage 4, with the amplitude in the middle of the nucleus now increasing as the domain walls grow radially. Lateral domain wall growth is even more pronounced in the PFM images at $t = 117$ μs, Stage 5, where the amplitude at the center of the switched domain has returned to the same contrast as the surrounding unswitched area, only its piezoresponse is completely out of phase. Only at this point is the new domain finally fully resolved.

Two other early stages of domain evolution (1a and 1b) are sketched in Fig. 4 but not assigned to image frames in Fig. 3. These possibilities are proposed elsewhere to describe PFM images where amplitude contrast reveals features but phase contrast does not.[77,87] Stage 1a refers to a "half ellipsoid" shaped domain that has initiated but not extended through the film thickness. This assumes that nucleation of the reverse domain occurs at a surface defect beneath the conducting AFM tip and the process follows the model proposed by Landauer,[120] where the geometry of the nucleated domain shape is approximately a half ellipsoid with radius r and length l. Applying the model with standard PZT parameters ($P_s = 0.40$ C/m^2, $\varepsilon = 100$, $\sigma_w = 0.132$ J/m^2)[80] and a maximum electric field value of 183 MV/m that could be applied in this work, the smallest critical nucleation size r^* is calculated to be ~ 1.8 nm (other models to approximate the nucleation size may yield a more accurate, but similarly minute, value[121]). This cannot be directly resolved, although as described above such sub-resolution features may just be detectable.

Alternatively, a nucleating but partial-thickness domain may grow laterally,[77] Stage 1b. However, given temporal steps on the order of microseconds and domain wall velocities around 1 mm/s observed here (and up to 50 m/s measured elsewhere with higher amplitude pulses,[122,123]), for the 30 nm thin film studied a partial-thickness domain would plausibly grow through the entire film thickness before it could be observed. The first appearance of contrast in amplitude images in this work is therefore attributed to through-thickness domains, Stage 2 in Fig. 4.

IV. Aerial Switching

The simplest application of this approach is to investigate the switched area during *in situ* poling, as occurs beneath an

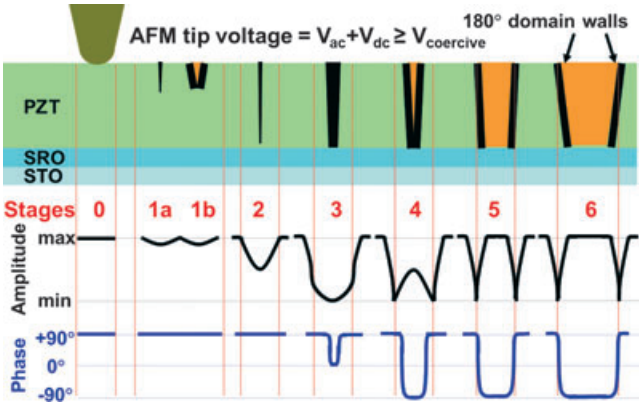

Fig. 4. Cross sectional diagram illustrating PFM amplitude and phase contrast for each step during the proposed process of domain nucleation, appearance in PFM signals, and growth, in accordance with the PFM images of Fig. 3.

electrode in a ferroelectric device. Fig 5 presents five images taken from a movie of several hundred frames during such switching from light to dark (4 μm on a side). The developing area of dark contrast, calculated for each image frame, is also plotted as a function of the cumulative poling time. This area is determined based on a simple threshold analysis of the image contrast, which is trivial for such essentially binary contrast. The experiment was then repeated twice, each with higher poling potentials. To monitor the relative influence of preexisting domain growth versus new domain nucleation, an initial 1 μm × 1 μm central feature (central dark box) was pre-poled as well. Interestingly, growth of the preexisting feature is essentially negligible, so that initially switching is almost equally slow regardless of the applied potential. After an apparent incubation time of ~ 50 μs, however, domain nucleation begins to occur, enabling far more rapid aerial switching for the highest applied biases.

V. Individual Domain Nucleation Times and Growth Velocities

Since HSSPM efficiently provides nanoscale resolution movies of domains nucleating and growing, this behavior can be quantified not just macroscopically as described above, but also for individual domains and with statistical rigor. As an example, a 2 μm × 2 μm region encompassing over 100 distinct domains was monitored during *in situ* switching following the same procedures as for Figs. 3 and 5. The montage

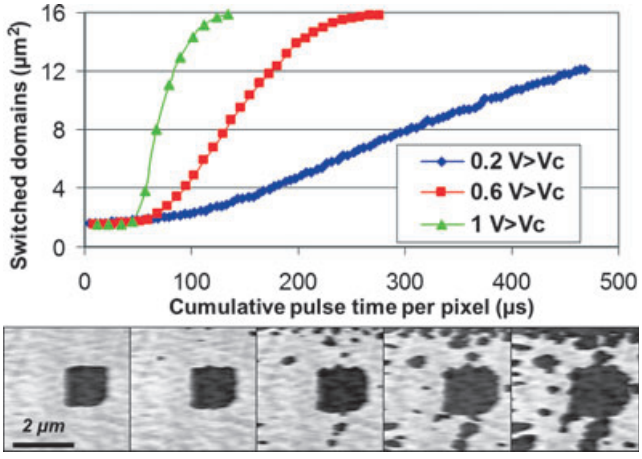

Fig. 5. Five 4 μm × 4 μm images (base) from a switching movie starting with a 1 μm × 1 μm prepoled box, allowing the overall switched area to be plotted (top) as a function of poling time for low, medium, and high biases beyond the coercive field.

of Fig. 6 presents 11 phase images from this movie, each acquired after 78 μs of cumulative poling per pixel, based on ~100 amplitude and phase frames. As in Fig. 3, nascent domains clearly develop, grow, and ultimately coalesce until nearly the entire field of view has switched (from light to dark contrast). To determine the size and location of every one of these features, frame by frame, feature tracking software was necessarily employed. Overall 171 individual domains were assessed, each distinctly identified, providing exceptional statistics for characterizing domain dynamics. The last pane in Fig. 6 identifies a subset of just 10 of these domains considered in greater detail below, each remaining isolated from its neighbors for at least 16 image frames so that nucleation and growth can be individually but comprehensively analyzed.

Figure 7(a) presents the domain area (in μm^2) for these 10 longest lasting domains as a function of cumulative poling time. The individual features are again determined based on simple binary contrast thresholds for each frame of Fig. 6, after which features at the same location from one frame to the next are linked as a single identifiable domain. Fig 7(b) plots the calculated radius for these domains. Note that with both Figs. 7(a) and (b), and for all other domains considered throughout this work, domains are only tracked while they are isolated to focus on the evolution of individual domains during ferroelectric switching. Since literally thousands of distinct domains can be investigated even in a single day of imaging given the high speed nature of these experiments, such analysis is automated wherever possible. This is typically achieved with the common and freely available software package ImageJ, and/or the more specialized program Improvision Volocity: Quantification. Practically, domains are only tracked until: (a) the detection of abrupt changes in area, radius, and/or centroid position, signifying coalescence with adjacent structures; or (b) intersection with image edges since a domain's extent beyond the scanned area, and thus the true size and shape, cannot be known.

Several important observations can be made about Figs. 7(a) and (b). Although macroscopic ferroelectric switching generally follows an exponential relation as described by Avrami-based phenomenological models,[124–126] the individual domains (and hundreds of others not shown for brevity) definitively grow linearly. Furthermore, switching progresses with great variability between individual domains, in terms of both nucleation times and growth rates, even though in some cases the features are only hundreds of nanometers apart. Variability at the periphery of each domain is common as well, addressed in a later section of this article.

As was first observed with the benefit of even better temporal resolution studies,[98] the growth velocities of nascent domains are significantly faster than mature domains. Indeed, the radius has been measured to climb 10 times faster for domains in the initial stages of growth, slowing down to more consistent linear growth only beyond a radius of 25–50 nm. Of course it is expected that polarization reversal will occur at a different speed for predominantly through-thickness switching as opposed to lateral domain wall movement, that is for stages 1–2, or stages 3–6, respectively, in Fig. 4. Since radius measurements for Fig. 7(b) are based on phase contrast, though (i.e., stages 3–6), lateral domain growth is expected to dominate for the compiled data. Therefore, a different explanation is more likely for the initially enhanced domain growth. Separate work suggests that defects present in the film lower the local activation energy for switching, and hence act as nucleation sites. These potential wells extend laterally on the order of 50 nm, beyond which domain walls slow down as they have climbed out of the potential well.

The domain wall velocity for each domain in Fig. 6 can be quantified based on the slopes of Fig. 7(b). Fig 8(a) presents a histogram of these extrinsic velocities, as well as 76 additional domains with the next greatest longevity from the

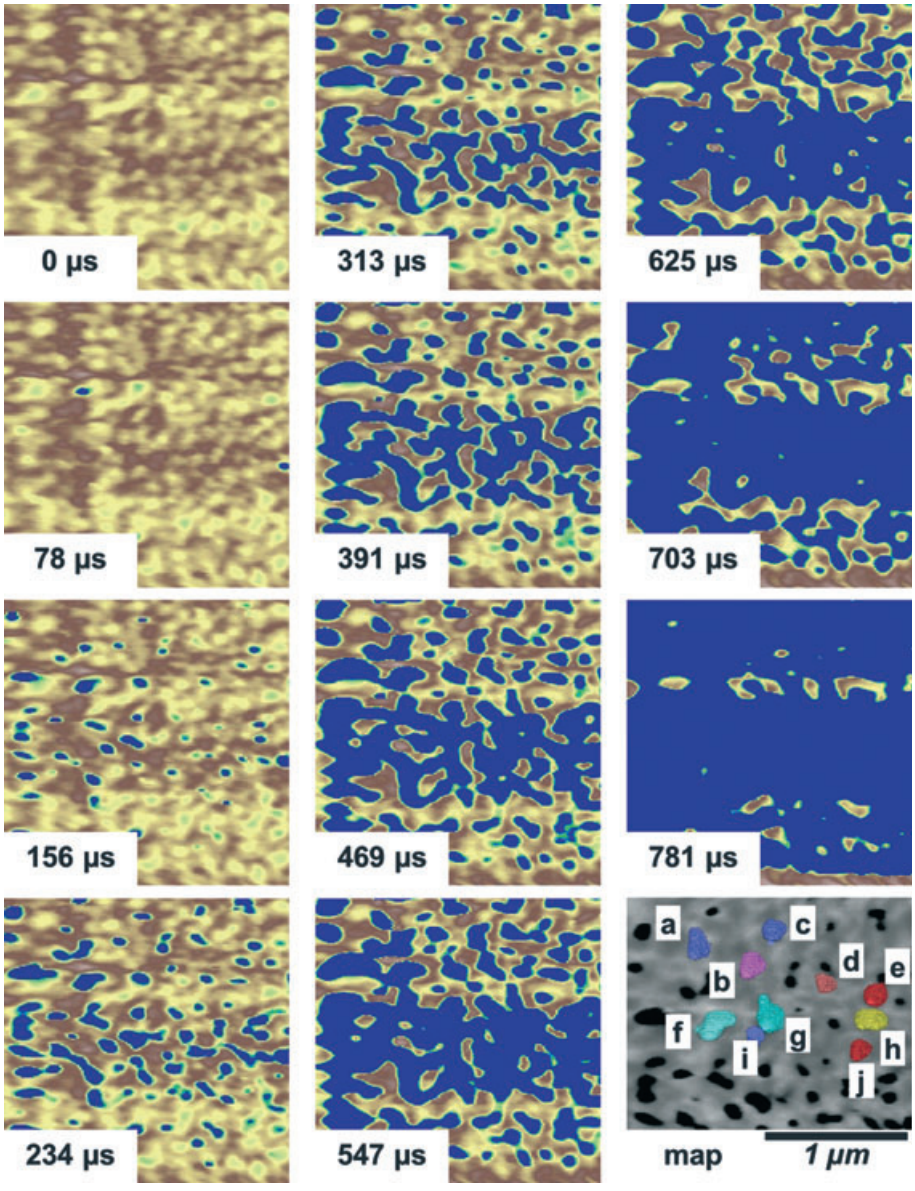

Fig. 6. Frames from a switching movie allowing individual domains to be tracked (the final frame highlights 10 of these domains for further analysis).

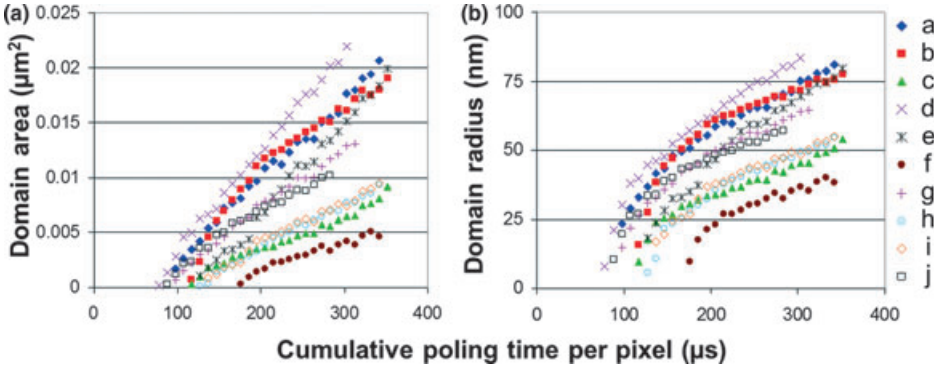

Fig. 7. Development of individual domain areas (left) and radii (right) for 10 distinct ferroelectric domains from Fig. 6.

switching movie (in fact more domains are present, but were not tracked through sufficient frames to meaningfully determine their velocity). The directly measured velocities range over an order of magnitude from 0.18 to 1.8 mm/s, with an average of 0.56 ± 0.36 mm/s (error indicates standard deviation). Based on this constant growth rate and the HSSPM temporal resolution, the smallest steps in radii resolvable between the successive images presented are ~ 5.5 nm. For comparison, the average minimum domain radius measured directly during switching is roughly 14 nm. Since the Landauer predicted critical nucleation radius for these experimental conditions is 1.8 nm, it is therefore reasonable to assume that

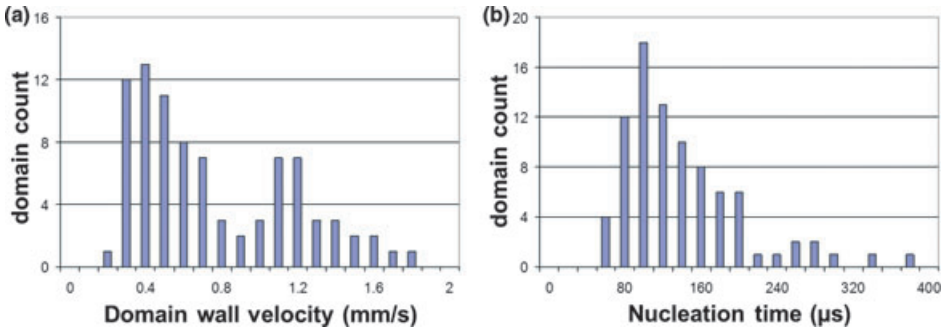

Fig. 8. Distribution of individual domain wall velocities, and nucleation times, determined from the switching movie of Fig. 6.

although the earliest stage of domain formation is not fully resolved as discussed with Fig. 4, nascent domains are experimentally observed within one to three image frames of their nucleation.

Accordingly, the domain-independent nucleation times have been estimated by linearly extrapolating the domain sizes from Fig. 7(a) back to an area of 0 μm^2. Fig 8(b) presents a histogram of these nucleation times, for the same domains as in Fig. 8(a). Like the domain wall velocities, the nucleation times also range over nearly an order of magnitude, from 45 to 372 μs, with an average of 132 ± 55 μs (standard deviation). The average spacing between nucleation sites is 147 ± 40 nm, although again tremendous variability is apparent. Clearly, uniform nucleation rates, growth velocities, and separations between domain sites do not occur, even though they are assumed by classical theories of ferroelectric domain switching.[124–126] It is important to note that the apparently long nucleation times, and slow domain wall velocities, are extrinsic values as they are exponentially proportional to the applied bias. If even larger voltages were employed instead, such as with Fig. 5, shorter nucleation times and higher velocities would be detected ultimately approaching their intrinsic values (sub-ns, and km/s, respectively). But since separate studies have shown that switching patterns are nearly identical over a range of biases,[98,127] low field approaches are ideal to quantify domain nucleation and growth with optimal spatial and temporal resolution.

Since the locations of each of the domains considered in Figs. 6–8 are known, nanoscale maps of individual domain nucleation times and growth rates can ultimately be prepared, Figs. 9(a) and (b), respectively. In total 86 independent domains are considered, each marked with an x in the figure. Between each of these sites the results are linearly interpolated, simply to guide the eye about general trends in the domain behavior from one location to the next. Beyond the boundary of the outer-most domain measurements, the arbitrary value of 0 has been entered since the surrounding landscape is not known.

Of course it is possible to extrapolate these maps to plot activation energies (E_a) for domain nucleation[59] and growth according to Eqs. (1) and (2), respectively. However, this requires further assumptions to be made, particularly of the intrinsic critical nucleation time ("t_∞") and growth rate for an infinite voltage ("velocity$_\infty$"). Individual domains simply have not yet been measured with the combination of sufficient spatial, temporal, and voltage resolution (simultaneously) that is necessary to know these terms for truly quantifying the individual activation energies, a focus of separate work.[127]

$$t_{\text{nucleation}} = t_{\infty,\text{nucleation}} * \exp\left(\frac{E_{\text{a,nucleation}}}{V_{\text{applied}}}\right) \quad (1)$$

$$\text{velocity}_{\text{growth}} = \text{velocity}_{\infty} * \exp\left(-\frac{E_{\text{a,growth}}}{V_{\text{applied}}}\right) \quad (2)$$

Several conclusions about relative activation energies can nevertheless be uniquely drawn from the results of Fig. 9. First, there is an extensive variation in nucleation times, and thus nucleation activation energies, as expected since this mechanism will depend primarily on individual defects and their corresponding local mechanical and electric field distortions. Second, although some domains exhibit a seemingly coupled low nucleation time (nucleation activation energy) and high growth rate (growth activation energy), upon considering all 86 measured domains these parameters are pre-

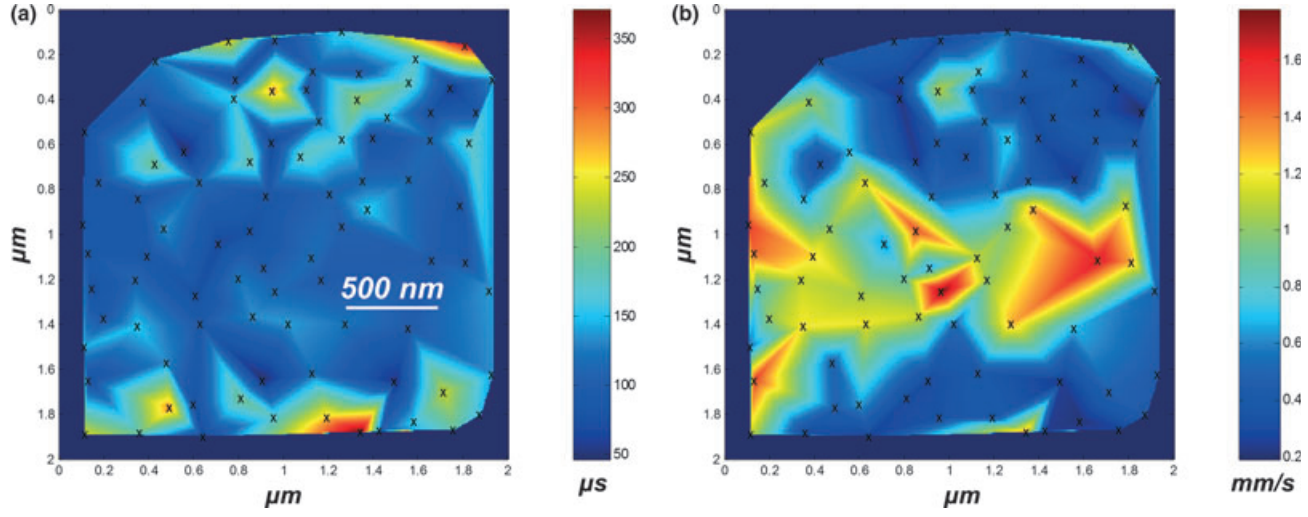

Fig. 9. Maps of domain wall velocities and nucleation times at nucleation sites identified by "x" markings (note: contrast is linearly interpolated between nucleation sites).

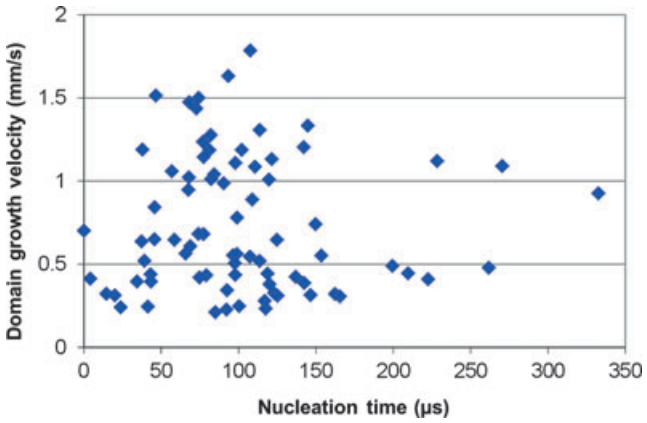

Fig. 10. Growth velocity plotted with respect to nucleation time for individual domains, revealing decoupling between nucleation and growth mechanisms.

dominantly disconnected, counter to traditional nucleation and growth models for crystallization. This point is especially clear when plotting growth velocity versus nucleation time, Fig. 10, where the results are seemingly arbitrarily scattered instead of correlated as anticipated from Eq. (3) (determined by assuming the nucleation and growth activation energies from Eqs. (1) and (2) can be equated).

$$\ln(\text{velocity}_{\text{growth}}) = -\ln(t_{\text{nucleation}}) + \left[\ln(\text{velocity}_{\infty}) + \ln(t_{\infty,\text{nucleation}})\right] \quad (3)$$

This disconnect is explained by the distinctly different mechanisms for domain nucleation and growth, including a relative lack of long-range coupling in ferroelectrics (e.g., as compared to ferromagnetics). Consequently, the activation energy to nucleate a new domain at a given defect site in the film is unlikely to influence the energy for switching at the domain's periphery, especially once the radius extends to hundreds of nanometers or more as measured here. The profound and decoupled variation measured for nucleation times and growth velocities may provide new strategies for optimizing device switching speeds and ferroelectric system reliability,[128] and clearly demonstrates the need to incorporate such parameters for accurate modeling of domain dynamics.

VI. Cycling Studies

Curiously, the growth rate appears to be more rapid in a band near the center of the images in Fig. 9, supported by inspecting Fig. 6 and the accompanying switching movies which reveal this region switching fastest. It is believed that this enhanced growth as compared to the surrounding area relates to previous poling in this region. Notably, however, the nucleation time is not nearly as strongly influenced, possibly providing evidence that domain imprint and/or fatigue most impact domain growth rates, and not domain nucleation times. To investigate this notion further, the conducting AFM probe was positioned in a single location and used to cycle the polarity as many as 10 000 times. The cycles were repeated at 10 Hz, requiring just under 17 min to complete for the most severe case, during which spatial drift of the tip position was less than the tip diameter (50–100 nm). Local PFM-based hysteresis loops were acquired before and after this cycling experiment, Fig. 11. Both the initial and the post loops shown are the average of 10 consecutive hysteresis measurements, with 95% confidence bars indicated. As

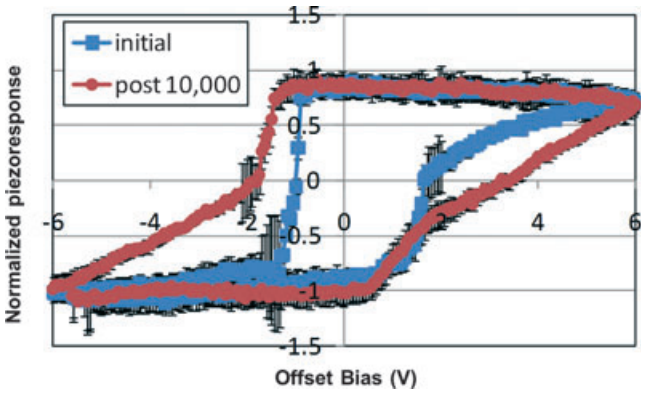

Fig. 11. Hysteresis loop before, and after, switching a single region 10 000 times.

expected, the onset of switching occurs at nearly the same applied bias for both polarization directions. It takes much higher voltages to complete polarization reversal after cycling, however, again possibly supporting the notion that growth is inhibited more than nucleation by switching fatigue.

The shapes of hysteresis loops have been carefully analyzed by other groups and interpreted as being related to the type, and depth, of defects beneath the probe.[97,129–132] Here, the dynamics of switching are additionally mapped by acquiring switching movies at the same location as the cycling studies following the point measurements. Fig. 12 presents a montage of image frames during polarization reversal in the vicinity of the 10 000 cycle measurement (identified with an arrow, lower right), as well as three other locations cycled 1000 times each (remaining arrow positions). The consecutive images, acquired in the same manner as in Figs. 3 and 6, reveal that the highest cycled region resists switching, becoming one of the last locations to switch, whereas switching movies before the cycling experiment revealed no such behavior.

Possible explanations for these observations are that repeated polarization may have caused ionic defect accumulation or depletion, not surprisingly impacting further switching dynamics. Of course film modification is also possible since the surface is not protected from the environment in these measurements. Equivalent HSSPM experiments conducted in vacuum would address this question but have not yet been performed, although it is likely based on evidence from standard PFM measurements in controlled environments[133] and/or vacuum.[134,135] In any case, this experiment is insightful as it demonstrates the application of HSSPM for investigating fatigue effects. While applied here to ferroelectrics, the method should be valid for studies of batteries, fuel cells, photovoltaics, thermoelectric, etc. where cycle-induced performance degradation (i.e., fatigue, burn-in, etc.) is also a concern.

VII. Ferroelectric Hysteresis Mapping

The hysteresis loops shown in Fig. 11 are for a single location, so they are indicative of the response of the material directly beneath the tip only. For real devices based on nano- to micro- sized electrodes, on the other hand, their polarization response represents the ensemble behavior of the entire area below the top electrode, several orders of magnitude larger than the contact area of an AFM tip. Such necessarily macroscopic measurements therefore cannot distinguish between a single domain growing rapidly, and many domains growing slowly but simultaneously. With HSSPM, this collective response can be directly visualized, since independent domains can be seen to nucleate, grow, and coalesce with their neighbors during acquisition of the hysteresis loop.

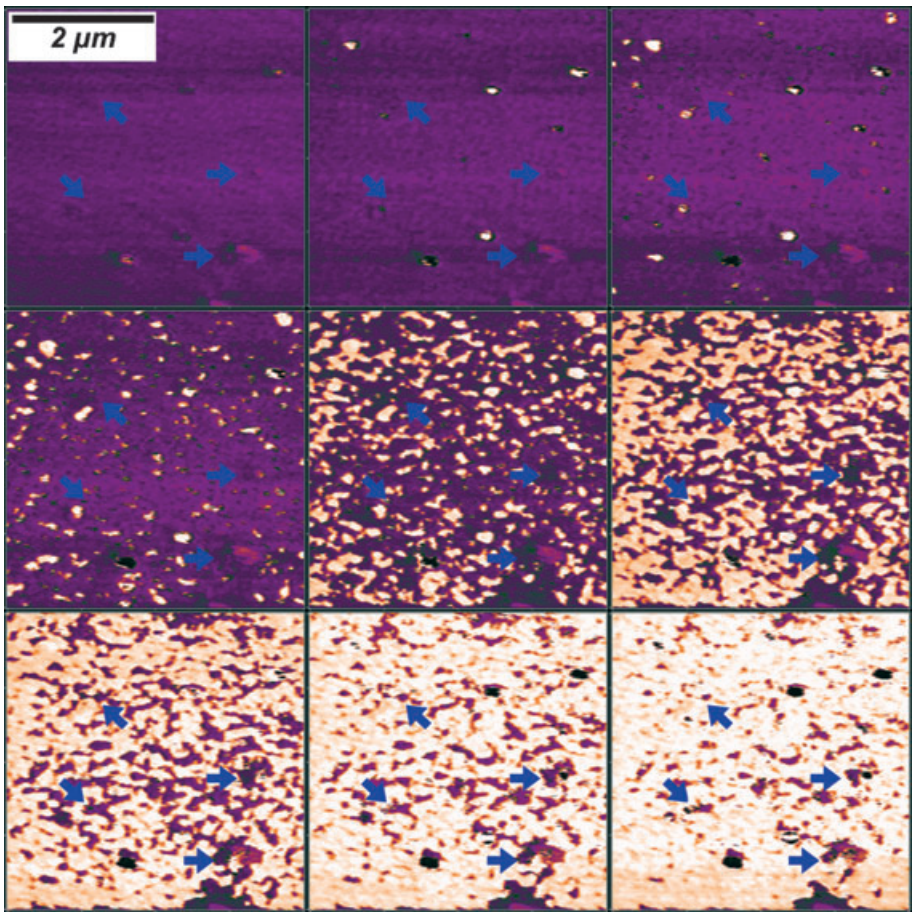

Fig. 12. Montage of images from a switching movie in the vicinity of four locations prepoled by 10 000 (indicated by arrow at lower right) or 1000 (other arrow positions) super-coercive-field voltage cycles.

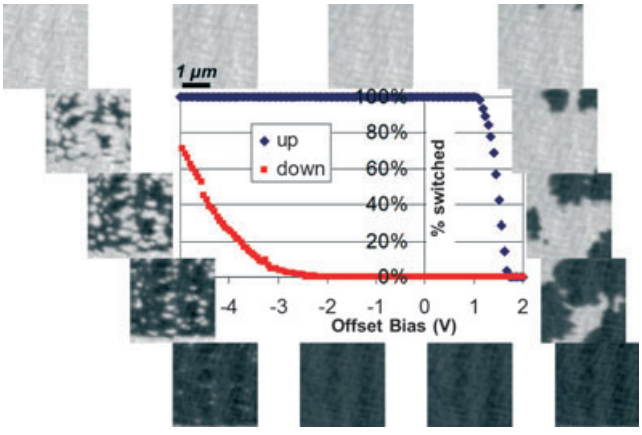

Fig. 13. Fourteen 3 μm × 3 μm frames from a switching movie acquired with each frame at a distinct DC bias, and the resulting hysteresis loop (enclosed) which can be determined based on the average image contrast for each frame.

Fig 13 presents such a "hysteresis movie", with 14 representative 3 μm × 3 μm images acquired during *in situ* poling, first increasing from −5 V (upper left) to +2 V (clockwise toward lower right), then decreasing back down to −5 V. A total of 256 such images were in fact collected, 3 s per image frame, where each image is for a slightly higher DC bias (+55 mV) when switching from negative up to positive, or an equally lower bias (−55 mV) when switching back down again. A subset of these images appears on the Journal's cover.

The encompassed plot presents the corresponding effective area hysteresis loop, where each data point indicates the percentage area switched for a single image in the hysteresis movie based on the average pixel contrast. The figure thus overlays the average extent of polarization reversal for what is essentially a 9 μm^2 capacitor, with the locally resolved actual domain response. The experiment began with a 100% backpoled surface, with a DC bias of −5 V, yielding uniform white PFM contrast. With each new image, the voltage was increased, although the contrast remained unchanged until reaching a DC bias of ~ +1 V. At this point, two domains (dark contrast) developed at nucleation sites in the upper right of the imaged area. These grew very rapidly as the DC bias continued to rise, combining with a handful of other nucleated domains before completely switching the entire imaged area at 1.67 V (fully reversed polarity).

As the voltage was next stepwise decreased during HSSPM, switching again did not commence for many images, with nucleation sites only beginning to be detected for a DC bias of ~ −2.5 V. Unlike for positive poling, however, this time polarization reversal proceeded over a much larger range of voltages. Conspicuously, the switching mechanism is also now dominated by domain nucleation instead of growth, with tens to hundreds of nucleation sites activated but their corresponding domains growing relatively slowly. The average hysteresis response is clearly strongly asymmetric, and could be measured as such with much simpler macroscopic or standard PFM measurements, but this approach allows the asymmetry to be directly coupled to the dynamic response as well.

Furthermore, since every pixel in each image in the hysteresis movie of Fig. 13 indicates the local domain orientation (with each frame representing a different offset voltage), local hysteresis loops can also be easily generated for each image position. This is practically achieved by simply extracting the piezoresponse for the pixel in the *i*th row and the *j*th column

in all 256 images in the dataset, and plotting these values versus the corresponding offset voltage for each distinct image. Accordingly, Fig. 14 presents a subset of 128 hysteresis loops, one for each pixel along a vertical line down the center of the switching movie. The variation in switching response is dramatic, with switching beginning at positive biases anywhere from 1 to 1.8 V, and negative biases between −3 and −5 V, a much broader range than indicated by the macroscopic response alone.

A wide range of parameters related to the hysteresis loop magnitude, voltage for onset or completion of switching, slope or curvature during switching, linearity of the response, etc. has been considered on numerous occasions, especially with the switching spectroscopy PFM method.[129] Similarly, Fig. 15 displays the hysteresis loop width at every image pixel from Fig. 13, some with loops as narrow as 3.5 V (dark contrast) and others as high as 6.5 V (bright). These values are determined simply based on the difference between the local switching potentials for up and down polarization from the loops as in Fig. 14, but considering all 128 000 loops acquired (one for each image pixel).

The major contributor to the observed variation in hysteresis widths is the heterogeneity in nucleation behavior in the negative poling direction. The abrupt switching by growth mechanisms for positive tip biases happens to contribute little to Fig. 15, since the variation from one location to another is relatively slight. Similar plots focused on other parameters that are characteristic of hysteresis loops, on the other hand, could obviously be profoundly different, and vary greatly with specimen, specimen position, local defects, etc.

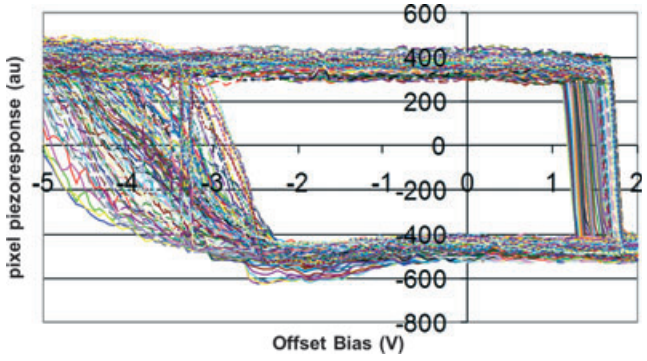

Fig. 14. 128 hysteresis loops extracted along a single column of pixels from the switching hysteresis movie from Fig. 13.

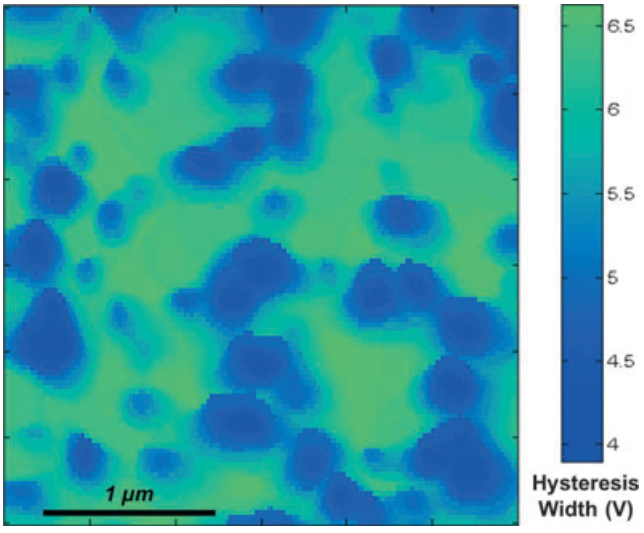

Fig. 15. Map of hysteresis widths (Volts) extracted from 128 000 distinct hysteresis loops acquired from the hysteresis movie of Fig. 13.

Interestingly, there is another way to consider the data from Fig. 13 which is insightful for understanding not just the nucleation site density, but also the energetics of these nucleation sites. The approach is to calculate the number of new domains which appear in each pixel frame, and therefore new domains as a function of increasing poling potential and/or time. Fig 16 presents the resulting histogram of such "new" domain formation, compared with the much higher "total" number of domains per image frame throughout the hysteresis movie. This reveals how many domains nucleate, and also how many coexist and/or coalesce, at any given stage in the switching process.

For convenience, the axes in Fig. 16 are swapped to highlight the applied bias versus the domain counts. This portrays the density as well as the energy of nucleation sites in a manner reminiscent of a classic density of states diagram. An analysis of such results for a range of specimens is forthcoming, but in this particular case nucleation sites are relatively uniformly distributed in energy, at least up to the voltage detected. It is noteworthy that higher energy nucleation sites surely exist as well, and in fact are known to do so from point by point hysteresis measurements.[97] However, these are simply never activated during areal polarization as in capacitive devices, since such locations switch via a more preferential mechanism than local nucleation—instead, an adjacent, lower activation energy site switches, and then expands by domain growth to consume surrounding positions. HSSPM thus allows the crucial growth mechanism and its interplay with nucleation to be directly and uniquely visualized, quantified, and mapped.

Local hysteresis loops acquired with area-switching measurements as in HSSPM therefore incorporate polarization due to either nucleation (if the location is actually a nucleation site), or to growth of a nearby domain. They provide the density of practically active nucleation sites, determine the real field necessary for switching at each location in the context of neighboring domain behavior, and allow the switching mechanism to be directly visualized (nucleation or growth). On the other hand, hysteresis loops acquired independently at each image pixel, one by one, are crucial to identify the breadth of activation energies within the specimen. Such point by point hysteresis measurements are therefore an excellent measure of film homogeneity in terms of nucleation, whereas area resolved switching measurements that record the ensemble switching behavior are strongly relevant to measures of device performance where collective nucleation and growth must be taken into account.

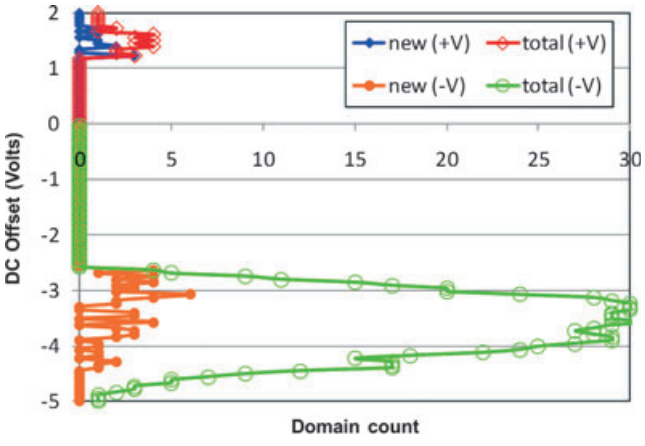

Fig. 16. Density of domain nucleation sites (overall, and new) from Fig. 13, plotted similar to a density of states diagram.

VIII. A Classic Approach

Interestingly, HSSPM results provide a fascinating opportunity to directly visualize an approach employed by Cahn for studies of transformation kinetics, the so called "time-cone method."[136] This concept elegantly builds on the widely applied Johnson–Mehl–Avrami–Kolmogorov (JMAK) model, providing transformation rates based on randomly distributed nucleation events in space and time.[137–141] It is applicable to ferroelectric switching via the Kolmogorov–Avrami–Ishibashi (KAI) model,[124,142] which also developed from JMAK theory.

The time-cone approach considers time as the third (z) axis for a planar specimen, with cones emanating upward from the location in x and y at which nucleation occurs.[143] The growth velocity evidently dictates the cone opening angle, and overlapping cones signify coalescing domains. Modifications of this model were developed to account for a continuous probability of nucleation events with poling time (i.e., a uniform density of nucleation states, and thus cones with their apices at a range of heights), or for a sudden burst of nucleation events (a delta-function density of states, causing multiple cones all with the same initial depth). A range of specimen geometries have also been considered from one to three dimensions, finite and infinite.

Accordingly, Fig. 17 depicts time cones such as those envisioned by Cahn, but resolved herein at the nanoscale. This is generated by plotting the switching time for each pixel from the dataset of Fig. 5 with color and rendered in three-dimensional (z-axis and color represents time). Bright, flat, and high regions did not switch during the experiment. Numerous time cones (domains) are apparent, and although comparisons to the analytical model are obvious, limitations of its elegant simplicity become clear as the lateral and vertical distribution of cone initiation points (locations and nucleation times, respectively), average opening angles (overall domain velocities), local slopes (local domain wall velocities around a single domain or cone), and overlapping patterns (coalescence) are directly measured. The variation is tremendous between domains, and for any given single domain.

IX. Switching and Defects

Although the results presented thus far have evidenced heterogeneities in the ferroelectric materials, presumably including point or clustered defects, dislocation sites, and/or even atomic steps in the underlying substrate, this section is concerned with more substantial features including grain boundaries and microcracks.

Grain boundaries are certainly present for many commercial ferroelectric applications due to the challenges in scaling up manufacturing of single crystal and/or epitaxial materials. But as individual device sizes continue to shrink, the number of grains per device may not be able to scale proportionally, increasing the importance of the switching response for certain populations of, or even distinct, grain boundaries. Of course grain boundaries have been investigated before with PFM,[144] including studies of domains extending beyond grain boundaries,[145] hysteresis loop acquisition at interfaces,[146] the piezoresponse for grains with dimensions in the nanoscale,[104,147] and the influence of grains[71,101,148] and grain boundaries[102,149–151] on coercive fields and domain formation.[152] Focusing on domain dynamics at such an interface, Fig. 18 presents consecutive images in a HSSPM switching movie at a PZT grain boundary. Switching obviously progresses predominantly by domain growth for this specimen, with an initial nucleation site in the lower left corner of the 1.25 μm × 5 μm region pictured. Growth is then rapid for eight image frames, until the domain wall becomes completely pinned by a grain boundary located down the center of each image. In fact, further domain wall motion is restrained for 70 more image frames during which an identical bias was continually applied (frame labels indicate the image count). If the field of view were of just a single grain, the entire region would have switched nearly 10 times earlier. However, the domain wall only escapes from the grain boundary when a higher DC bias is applied to the tip at frame 102, after which polarization reversal rapidly completes for the entire field of view. Of course domain dynamics may not be so severely impacted by all grain boundaries, but undoubtedly interfaces can profoundly degrade the statistical distribution of switching speeds in polycrystalline ferroelectrics, a very real industrial challenge when countable numbers of grains are present in individual devices.

More severely, microcracks represent a worst-case scenario for industrial applications of ferroelectrics. However, the strain relief achieved by such a crack provides an interesting

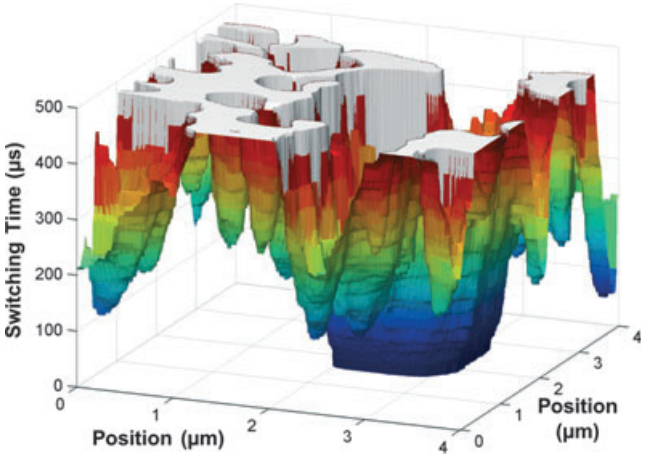

Fig. 17. Time-cone representation of ferroelectric polarization reversal, presenting the switching times from the movie of Fig. 5 with time defining the z-axis and contrast. Individual cones (domains) appear (nucleate) according to their nucleation times, growing (opening) with time but clearly in a much more complex manner than is assumed in classic and widely applied analytical approaches.

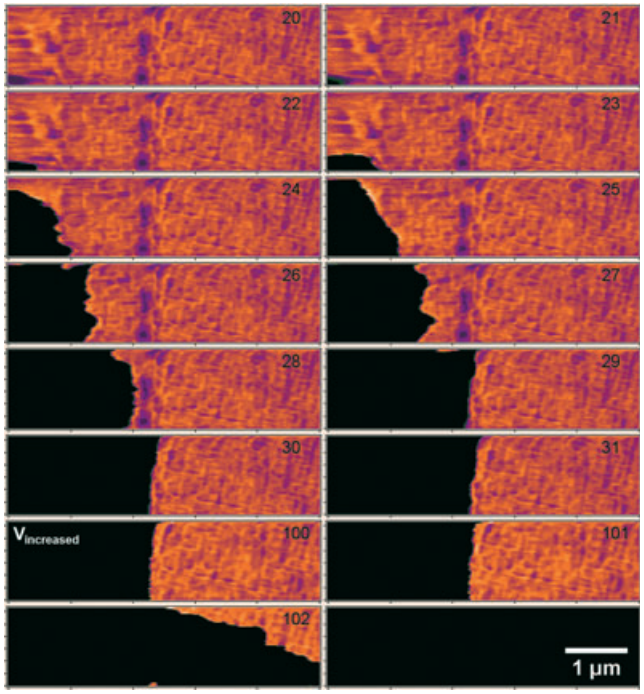

Fig. 18. HSSPM images (1.5 μm × 6 μm) during switching at a grain boundary, completely pinning the domain wall until the voltage is increased as identified.

platform to study the influence of local strain on switching dynamics. Such insight is otherwise difficult to acquire without employing strain stages[153], multiple specimens epitaxially grown on various substrates,[154–156] more macroscopic measurements, or testing as a function of temperature leveraging mismatches in thermal expansion coefficients. In each of these examples, however, additional complexities could mask the strain effects of interest. Accordingly, epitaxial specimens were indented with a diamond nanoindenter tip, creating sites of plastic deformation with microcracks emanating from their corners. HSSPM was then employed to monitor polarization reversal in the vicinity of the crack tips.

Before HSSPM was even performed, poling was induced at and around the indentation sites by the nanoindentation process itself due to the piezoelectric effect. Fig. 19 presents frames from a switching movie that followed, where nucleation and growth are inhibited at the crack location identified by the dotted line. Separate measurements indicate that just beyond the crack apex polarization is sometimes inhibited, and other times enhanced, with the opposite behavior along the edges of the crack. These observations are in excellent agreement with several theoretical studies,[157,158] which are otherwise difficult to experimentally investigate due to practical limitations on strain control and spatial and temporal resolution.

X. Future Opportunities

The conclusions one can draw from the various applications of HSSPM presented herein have inspired several additional avenues of investigation. For instance, the methods are easily extendable to in-plane piezoresponse imaging, enabling dynamics studies for more complex specimens and switching behavior than for epitaxial PZT systems such as $BiFeO_3$ films.[159] Studies of specimens with known point or line defects would yield important fundamental results on the interplay between certain defect geometries and nucleation and growth processes. Measurements on samples encompassing a range of thicknesses, compositions, and/or processing conditions would also be valuable academically and industrially. Strategies to optimize switching speeds and efficiency also come to mind, leveraging the advantages provided by numerous nucleation sites and the rapid growth of the ensemble of independent domains that result.[160]

Equivalent measurements on completely different ceramic systems are feasible as well, based on the sensitivity and *in situ* compatibility of SPM with electric and magnetic fields, mechanical properties, optical illumination, and thermal control. These present a wealth of further opportunities for fundamental and applied research, such as with multiferroics, thermoelectric, photovoltaics, and fuel cells, potentially providing insight into a wide range of fundamental and practical challenges in dynamic materials behavior at the nanoscale.

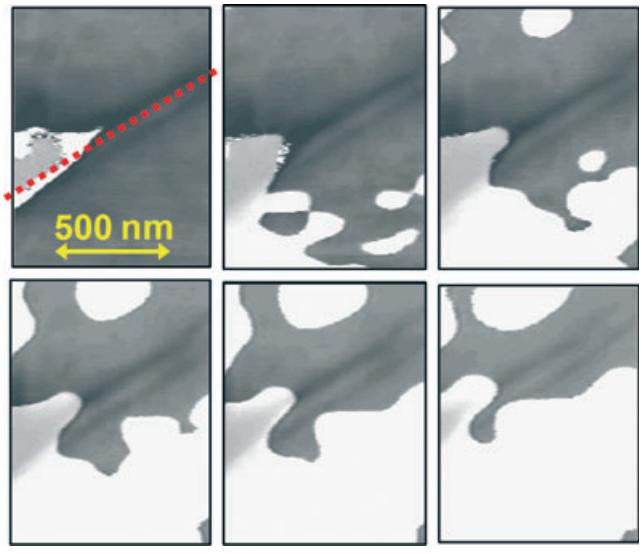

Fig. 19. Indentation-induced crack tip influencing domain nucleation and growth.

XI. Conclusion

The advent of High Speed Scanning Property Mapping provides unique opportunities for research into the dynamic properties of materials at the nanoscale. In this case ferroelectric domain switching in PZT thin films is tracked with microsecond temporal resolution by biasing the scanning probe just beyond the coercive field and simultaneously measuring the local domain orientation as it evolves. The development of nascent domains is directly revealed through movies of hundreds of consecutive images, acquired at line scanning rates as fast as 256 Hz, i.e., 1 frame per second. Individual domain nucleation times, and growth velocities, can thereby be uniquely quantified and mapped, identifying a wide variation in each contrary to typical theories of ferroelectric switching. The results further suggest that although the activation energies for domain nucleation and growth are uncorrelated, they are independently strongly coupled to macroscopic defects such as fatigue sites, grain boundaries, and microcracks. Combining high speed imaging with *in situ* activation thereby provides a novel means to investigate surface dynamics at the nanoscale, extendible through controlling voltage, magnetic fields, light, or temperature to a wide range of ceramic systems.

Acknowledgments

This work was partially supported by the National Science Foundation, Division of Materials Research, IMR award number 0817263. Specimens from Ying-Hao Chu, National Chiao Tung University, and Pu Yu and Ramamoorthy Ramesh, UC Berkeley are greatly appreciated.

References

[1]G. Binnig, C. F. Quate, and C. Gerber, "Atomic Force Microscope," *Phys. Rev. Lett.*, **56** [9] 930 (1986).

[2]D. A. Bonnell and B. D. Huey, "Basic Principles of Scanning Probe Microscopy"; pp. 8–42 in *Scanning Probe Microscopy & Spectroscopy: Theory, Techniques, and Applications*, Edited by D. A. Bonnell. Wiley-VCH, New York, 2001.

[3]S. R. Manalis, S. C. Minne, and C. F. Quate, "Atomic Force Microscopy for High Speed Imaging Using Cantilevers with an Integrated Actuator and Sensor," *Appl. Phys. Lett.*, **68** [6] 871–3 (1996).

[4]T. Sulchek, R. Hsieh, J. D. Adams, S. C. Minne, C. F. Quate, and D. M. Adderton, "High-Speed Atomic Force Microscopy in Liquid," *Rev. Sci. Instrum.*, **71** [5] 2097–9 (2000).

[5]P. Vettiger, M. Despont, U. Drechsler, U. Durig, W. Haberle, M. I. Lutwyche, H. E. Rothuizen, R. Stutz, R. Widmer, and G. K. Binnig, "The "Millipede" – More Than one Thousand Tips for Future AFM Data Storage," *IBM J. Res. Dev.*, **44** [3] 323–40 (2000).

[6]H. Kawakatsu, S. Kawai, D. Saya, M. Nagashio, D. Kobayashi, H. Toshiyoshi, and H. Fujita, "Towards Atomic Force Microscopy up to 100 MHz," *Rev. Sci. Instrum.*, **73** [6] 2317–20 (2002).

[7]T. Ando, N. Kodera, Y. Naito, T. Kinoshita, K. Furuta, and Y. Y. Toyoshima, "A High-Speed Atomic Force Microscope for Studying Biological Macromolecules in Action," *Chemphyschem*, **4** [11] 1196–202 (2003).

[8]J. Kwon, J. Hong, Y. S. Kim, D. Y. Lee, K. Lee, S. M. Lee, and S. I. Park, "Atomic Force Microscope with Improved Scan Accuracy, Scan Speed, and Optical Vision," *Rev. Sci. Instrum.*, **74** [10] 4378–83 (2003).

[9]T. J. McMaster, D. Brayshaw, M. J. Miles, A. E. Walsby, and P. Dunton, "A new Ultra High Speed AFM Technique for Biophysics: 3-Dimensional Imaging of Surfaces, Molecules and Processes with True Millisecond Resolution," *Biophys. J.*, **88** [1] 541A–41A (2005).

[10]Y. L. He, D. X. Zhang, and H. J. Zhang, "A Novel Atomic Force Microscope with High Stability and Scan Speed," *Instrum. Sci. Technol.*, **34** [5] 547–54 (2006).

[11]T. Ando, T. Uchihashi, N. Kodera, D. Yamamoto, M. Taniguchi, A. Miyagi, and H. Yamashita, "High-Speed Atomic Force Microscopy for Observing Dynamic Biomolecular Processes," *J. Mol. Recognit.*, **20** [6] 448–58 (2007).

[12]Y. G. Cui, Y. Arai, T. Asai, B. G. Ju, and W. Gao, "A High-Speed Atomic Force Microscope for Precision Measurement of Microstructured Surfaces," *Int. J. Precis. Eng. Manuf.*, **9** [3] 27–32 (2008).

[13]Y. J. Li, N. Kobayashi, H. Nomura, Y. Naitoh, M. Kageshima, and Y. Sugawara, "High-Speed Phase-Modulation Atomic Force Microscopy in Con-

stant-Amplitude Mode Capable of Simultaneous Measurement of Topography and Energy Dissipation," *Jpn. J. Appl. Phys.*, **47** [7] 6121–4 (2008).
[14]L. M. Picco, P. G. Dunton, A. Ulcinas, D. J. Engledew, O. Hoshi, T. Ushiki, and M. J. Miles, "High-Speed AFM of Human Chromosomes in Liquid," *Nanotechnology*, **19** [38] 384018 (2008).
[15]Y. Yan, Y. Wu, Q. Z. Zou, and C. M. Su, "An Integrated Approach to Piezoactuator Positioning in High-Speed Atomic Force Microscope Imaging," *Rev. Sci. Instrum.*, **79** [7] 073704 (2008).
[16]S. Bashash, R. Saeidpourazar, and N. Jalili, "Development, Analysis and Control of a High-Speed Laser-Free Atomic Force Microscope," *Rev. Sci. Instrum.*, **81** [2] 023707 (2010).
[17]C. Braunsmann and T. E. Schaffer, "High-Speed Atomic Force Microscopy for Large Scan Sizes Using Small Cantilevers," *Nanotechnology*, **21** [22] 225705 (2010).
[18]F. C. Tabak, E. C. M. Disseldorp, G. H. Wortel, A. J. Katan, M. B. S. Hesselberth, T. H. Oosterkamp, J. W. M. Frenken, and W. M. van Spengen, "MEMS-Based Fast Scanning Probe Microscopes," *Ultramicroscopy*, **110** [6] 599–604 (2010).
[19]R. C. Barrett and C. F. Quate, "High-Speed, Large-Scale Imaging with the Atomic Force Microscope," *J. Vac. Sci. Technol. B*, **9** [2] 302–6 (1991).
[20]T. Ando, N. Kodera, E. Takai, D. Maruyama, K. Saito, and A. Toda, "A High-Speed Atomic Force Microscope for Studying Biological Macromolecules," *Proc. Natl. Acad. Sci. USA*, **98** [22] 12468–72 (2001).
[21]T. Ando, D. Maruyama, K. Saito, and T. Toda, "The High-Speed AFM and Motion Pictures," *Biophys. J.*, **80** [1] 1257 (2001).
[22]J. K. Hobbs, C. Vasilev, and A. D. L. Humphris, "VideoAFM – A New Tool for High Speed Surface Analysis," *Analyst*, **131** [2] 251–6 (2006).
[23]B. D. Huey, "AFM and Acoustics: Fast, Quantitative Nanomechanical Mapping," *Annu. Rev. Mater. Res.*, **37**, 351–85 (2007).
[24]S. Morita, H. Yamada, and T. Ando, "Japan AFM Roadmap 2006," *Nanotechnology*, **18** [8] 1–10 (2007).
[25]L. M. Picco, L. Bozec, A. Ulcinas, D. J. Engledew, M. Antognozzi, M. A. Horton, and M. J. Miles, "Breaking the Speed Limit with Atomic Force Microscopy," *Nanotechnology*, **18** [4] 044030 (2007).
[26]G. Schitter and M. J. Rost, "Scanning Probe Microscopy at Video-Rate," *Mater. Today*, **11**, 40–8 (2008).
[27]Z. C. Li, E. Lee, and F. Ben Amara, "Performance Enhancement in High-Speed Contact-Mode Atomic Force Microscopy," *IEEE Trans. Contr. Syst. Technol.*, **17** [5] 1193–201 (2009).
[28]A. J. Fleming, B. J. Kenton, and K. K. Leang, "Bridging the gap Between Conventional and Video-Speed Scanning Probe Microscopes," *Ultramicroscopy*, **110** [9] 1205–14 (2010).
[29]A. D. L. Humphris, B. Zhao, D. Catto, J. P. Howard-Knight, P. Kohli, and J. K. Hobbs, "High Speed Nano-Metrology," *Rev. Sci. Instrum.*, **82** [4] 043710 (2011).
[30]R. Nath, Y.-H. Chu, N. A. Polomoff, R. Ramesh, and B. D. Huey, "High Speed Piezoresponse Force Microscopy: >1 Frame Per Second Nanoscale Imaging," *Appl. Phys. Lett.*, **93** [7] 072905–3 (2008).
[31]O. Kolosov and K. Yamanaka, "Nonlinear Detection of Ultrasonic Vibrations in an Atomic Force Microscope," *Jpn. J. Appl. Phys., Part 2 (Lett.)*, **32** [8A] 1095 (1993).
[32]U. Rabe and W. Arnold, "Acoustic Microscopy by Atomic-Force Microscopy," *Appl. Phys. Lett.*, **64** [12] 1493–5 (1994).
[33]K. Yamanaka, H. Ogiso, and O. Kolosov, "Ultrasonic Force Microscopy for Nanometer Resolution Subsurface Imaging," *Appl. Phys. Lett.*, **64** [2] 178–80 (1994).
[34]B. D. Huey, D. Lisjak, and D. A. Bonnell, "Nanometer-Scale Variations in Interface Potential by Scanning Probe Microscopy," *J. Am. Ceram. Soc.*, **82** [7] 1941–4 (1999).
[35]K. B. Crozier, G. G. Yaralioglu, F. L. Degertekin, J. D. Adams, S. C. Minne, and C. F. Quate, "Thin Film Characterization by Atomic Force Microscopy at Ultrasonic Frequencies," *Appl. Phys. Lett.*, **76** [14] 1950–2 (2000).
[36]B. Altemus, G. Shekhawat, X. Bai, R. E. Geer, and J. Castracane, "Nanoscale Elastic Imaging of Micro-Electro-Mechanical System Based Micromirrors," *Proc. SPIE – Int. Soc. Opt. Eng. (USA)*, **4558**, 143 (2002).
[37]B. D. Huey, "Ultrasonic Force Microscopy: Nanometer Scale Mechanical Contrast"; pp. 183–89 in *Acoustical Imaging*, Edited by R. G. Maev. Kluwer, New York, 2002.
[38]U. Rabe, M. Kopycinska, S. Hirsekorn, J. M. Saldana, G. A. Schneider, and W. Arnold, "High-Resolution Characterization of Piezoelectric Ceramics by Ultrasonic Scanning Force Microscopy Techniques," *J. Phys. D – Appl. Phys.*, **35** [20] 2621–35 (2002).
[39]M. Kopycinska, C. Ziebert, H. Schmitt, U. Rabe, S. Hirsekorn, and W. Arnold, "Nanoscale Imaging of Elastic and Piezoelectric Properties of Nanocrystalline Lead-Calcium Titanate," *Surf. Sci.*, **532**, 450–5 (2003).
[40]M. Salmeron, G. Neubauer, A. Folch, M. Tomitori, D. F. Ogletree, and P. Sautet, "Viscoelastic and Electrical-Properties of Self-Assembled Monolayers on Au(111) Films," *Langmuir*, **9** [12] 3600–11 (1993).
[41]K. Wadu-Mesthrige, N. A. Amro, J. C. Garno, S. Cruchon-Dupeyrat, and G. Y. Liu, "Contact Resonance Imaging – A Simple Approach to Improve the Resolution of AFM for Biological and Polymeric Materials," *Appl. Surf. Sci.*, **175**, 391–8 (2001).
[42]B. D. Huey, "SPM Measurements of Ferroelectrics at MHZ Frequencies"; pp. 239–62 in *Nanoscale Phenomena in Ferroelectric Thin Films*, Edited by S. Hong. Kluwer, Boston, MA, 2004.
[43]S. Jesse, B. Mirman, and S. V. Kalinin, "Resonance Enhancement in Piezoresponse Force Microscopy: Mapping Electromechanical Activity, Contact Stiffness, and Q Factor," *Appl. Phys. Lett.*, **89** [2] 022906 (2006).
[44]A. D. L. Humphris, M. J. Miles, and J. K. Hobbs, "A Mechanical Microscope: High-Speed Atomic Force Microscopy," *Appl. Phys. Lett.*, **86** [3] 034106 (2005).
[45]P. K. Hansma, G. Schitter, G. E. Fantner, and C. Prater, "High-Speed Atomic Force Microscopy," *Science*, **314** [5799] 601–2 (2006).
[46]O. Kolosov, A. Gruverman, J. Hatano, K. Takahashi, and H. Tokumoto, "Nanoscale Visualization and Control of Ferroelectric Domains by Atomic-Force Microscopy," *Phys. Rev. Lett.*, **74** [21] 4309–12 (1995).
[47]O. Auciello, A. Gruverman, H. Tokumoto, S. A. Prakash, S. Aggarwal, and R. Ramesh, "Nanoscale Scanning Force Imaging of Polarization Phenomena in Ferroelectric Thin Films," *MRS Bull.*, **23** [1] 33–42 (1998).
[48]A. Gruverman, O. Auciello, and H. Tokumoto, "Imaging and Control of Domain Structures in Ferroelectric Thin Films Via Scanning Force Microscopy," *Annu. Rev. Mater. Sci.*, **28** [1] 101–23 (1998).
[49]C. Dehoff, B. J. Rodriguez, A. I. Kingon, R. J. Nemanich, A. Gruverman, and J. S. Cross, "Atomic Force Microscopy-Based Experimental Setup for Studying Domain Switching Dynamics in Ferroelectric Capacitors," *Rev. Sci. Instrum.*, **76** [2] 023708 (2005).
[50]S. Jesse, A. P. Baddorf, and S. V. Kalinin, "Switching Spectroscopy Piezoresponse Force Microscopy of Ferroelectric Materials," *Appl. Phys. Lett.*, **88** [6] 062908 (2006).
[51]N. Balke, I. Bdikin, S. V. Kalinin, and A. L. Kholkin, "Electromechanical Imaging and Spectroscopy of Ferroelectric and Piezoelectric Materials: State of the Art and Prospects for the Future," *J. Am. Ceram. Soc.*, **92** [8] 1629–47 (2009).
[52]D. A. Bonnell, S. V. Kalinin, A. L. Kholkin, and A. Gruverman, "Piezoresponse Force Microscopy: A Window into Electromechanical Behavior at the Nanoscale," *MRS Bull.*, **34** [9] 648–57 (2009).
[53]A. Gruverman, "Nanoscale Insight Into the Statics and Dynamics of Polarization Behavior in Thin Film Ferroelectric Capacitors," *J. Mater. Sci.*, **44** [19] 5182–8 (2009).
[54]S. V. Kalinin, A. N. Morozovska, L. Q. Chen, and B. J. Rodriguez, "Local Polarization Dynamics in Ferroelectric Materials," *Rep. Prog. Phys.*, **73** [5] 056502 (2010).
[55]S. M. Yang, J. G. Yoon, and T. W. Noh, "Nanoscale Studies of Defect-Mediated Polarization Switching Dynamics in Ferroelectric Thin Film Capacitors," *Curr. Appl. Phys.*, **11** [5] 1111–25 (2011).
[56]M. Alexe and A. Gruverman, *Nanoscale Characterisation of Ferroelectric Materials: Scanning Probe Microscopy Approach*. Springer Verlag, Berlin, 2004.
[57]S. Hong, *Nanoscale Phenomena in Ferroelectric Thin Films*. Kluwer, Dordrecht, The Netherlands, 2004.
[58]S. V. Kalinin and A. Gruverman, *Scanning Probe Microscopy of Functional Materials: Nanoscale Imaging and Spectroscopy*. Springer, New York, 2010.
[59]W. J. Merz, "Domain Formation and Domain Wall Motions in Ferroelectric $BaTiO_3$ Single Crystals," *Phys. Rev.*, **95** [3] 690–8 (1954).
[60]J. Munoz-Saldana, G. A. Schneider, and L. M. Eng, "Stress Induced Movement of Ferroelastic Domain Walls in $BaTiO_3$ Single Crystals Evaluated by Scanning Force Microscopy," *Surf. Sci.*, **480** [1–2] L402–10 (2001).
[61]H. Fujisawa, M. Shimizu, and H. Niu, "Piezoresponse Force Microscopy Observations of Switching Behavior in Pb(Zr,Ti)O-3 Capacitors," *Jpn. J. Appl. Phys. Part 1 - Regul. Pap. Short Notes Rev. Pap.*, **43** [9B] 6571–5 (2004).
[62]B. Lee, C. Bae, S. H. Kim, and H. Shin, "Characterization of Self-Assembling Isolated Ferroelectric Domains by Scanning Force Microscopy," *Ultramicroscopy*, **100** [3–4] 339–46 (2004).
[63]P. Paruch, T. Tybell, T. Giamarchi, and J. M. Triscone, "Nanoscopic Studies of Disorder-Controlled Static and Dynamic Properties of Domain Walls in Epitaxial Ferroelectric Films," *Abstr. Pap. Am. Chem. Soc.*, **230**, 88-PHYS (2005).
[64]A. Agronin, M. Molotskii, Y. Rosenwaks, G. Rosenman, B. J. Rodriguez, A. I. Kingon, and A. Gruverman, "Dynamics of Ferroelectric Domain Growth in the Field of Atomic Force Microscope," *J. Appl. Phys.*, **99** [10] 104102 (2006).
[65]T. K. Song, Y. W. So, D. J. Kim, J. Y. Jo, and T. W. Noh, "Ferroelectric Switching Dynamics and Pulse-Switching Polarization Measurements," *Integr. Ferroelectr.*, **78**, 191–7 (2006).
[66]F. Zavaliche, S. Y. Yang, T. Zhao, Y. H. Chu, M. P. Cruz, C. B. Eom, and R. Ramesh, "Multiferroic $BiFeO_3$ Films: Domain Structure and Polarization Dynamics," *Phase Transitions*, **79** [12] 991–1017 (2006).
[67]J. Y. Jo, H. S. Han, J. G. Yoon, T. K. Song, S. H. Kim, and T. W. Noh, "Domain Switching Kinetics in Disordered Ferroelectric Thin Films," *Phys. Rev. Lett.*, **99** [26] 267602 (2007).
[68]B. J. Rodriguez, S. Jesse, J. Kim, S. Ducharme, and S. V. Kalinin, "Local Probing of Relaxation Time Distributions in Ferroelectric Polymer Nanomesas: Time-Resolved Piezoresponse Force Spectroscopy and Spectroscopic Imaging," *Appl. Phys. Lett.*, **92** [23] 232903 (2008).
[69]L. H. Wang, J. Yu, Z. H. Wang, H. Z. Zeng, Y. B. Wang, and J. X. Gao, "*In Situ* Investigation of Retention Properties of Polydomain Ferroelectric Thin Films by Multimode Scanning Force Microscopy," *Integr. Ferroelectr.*, **98**, 26–34 (2008).
[70]Y. Kim, H. Han, W. Lee, S. Baik, D. Hesse, and M. Alexe, "Non-Kolmogorov-Avrami-Ishibashi Switching Dynamics in Nanoscale Ferroelectric Capacitors," *Nano Lett.*, **10** [4] 1266–70 (2010).

[71]V. V. Shvartsman and A. L. Kholkin, "Investigation of the Ferroelectric-Relaxor Transition in $PbMg1/3Nb_2/3O_3$-$PbTiO_3$ Ceramics by Piezoresponse Force Microscopy," *J. Appl. Phys.*, **108** [4] 042007 (2010).

[72]H. Bea, B. Ziegler, M. Bibes, A. Barthelemy, and P. Paruch, "Nanoscale Polarization Switching Mechanisms in Multiferroic $BiFeO_3$ Thin Films," *J. Phys.-Condes. Matter*, **23** [14] 142201 (2011).

[73]T. H. Kim, S. H. Baek, S. M. Yang, Y. S. Kim, B. C. Jeon, D. Lee, J. S. Chung, C. B. Eom, J. G. Yoon, and T. W. Noh, "Polarity-Dependent Kinetics of Ferroelectric Switching in Epitaxial BiFeO3(111) Capacitors," *Appl. Phys. Lett.*, **99** [1] 012905 (2011).

[74]A. Roelofs, U. Bottger, R. Waser, F. Schlaphof, S. Trogisch, and L. M. Eng, "Differentiating 180 Degrees and 90 Degrees Switching of Ferroelectric Domains with Three-Dimensional Piezoresponse Force Microscopy," *Appl. Phys. Lett.*, **77** [21] 3444–6 (2000).

[75]C. S. Ganpule, A. L. Roytburd, V. Nagarajan, B. K. Hill, S. B. Ogale, E. D. Williams, R. Ramesh, and J. F. Scott, "Polarization Relaxation Kinetics and 180 Degrees Domain Wall Dynamics in Ferroelectric Thin Films," *Phys. Rev. B*, **65** [1] 014101 (2002).

[76]P. Paruch, T. Giamarchi, and J. M. Triscone, "Domain Wall Roughness in Epitaxial Ferroelectric $PbZr_{0.2}Ti_{0.8}O_3$ Thin Films," *Phys. Rev. Lett.*, **94** [19] 197601 (2005).

[77]S. Hong, E. L. Colla, E. Kim, D. V. Taylor, A. K. Tagantsev, P. Muralt, K. No, and N. Setter, "High Resolution Study of Domain Nucleation and Growth During Polarization Switching in Pb(Zr,Ti)O-3 Ferroelectric Thin Film Capacitors," *J. Appl. Phys.*, **86** [1] 607–13 (1999).

[78]T. Tybell, P. Paruch, T. Giamarchi, and J. M. Triscone, "Domain Wall Creep in Epitaxial Ferroelectric $Pb(Zr_{0.2}Ti_{0.8})O_3$ Thin Films," *Phys. Rev. Lett.*, **89** [9] 097601 (2002).

[79]A. Gruverman, B. J. Rodriguez, C. Dehoff, J. D. Waldrep, A. I. Kingon, R. J. Nemanich, and J. S. Cross, "Direct Studies of Domain Switching Dynamics in Thin Film Ferroelectric Capacitors," *Appl. Phys. Lett.*, **87** [8] 082902 (2005).

[80]P. Paruch, T. Giamarchi, T. Tybell, and J. M. Triscone, "Nanoscale Studies of Domain Wall Motion in Epitaxial Ferroelectric Thin Films," *J. Appl. Phys.*, **100** [5] 051608 (2006).

[81]D. J. Kim, J. Y. Jo, T. H. Kim, S. M. Yang, B. Chen, Y. S. Kim, and T. W. Noh, "Observation of Inhomogeneous Domain Nucleation in Epitaxial Pb $(Zr,Ti)O_3$ Capacitors," *Appl. Phys. Lett.*, **91** [13] 132903 (2007).

[82]S. M. Yang, J. Y. Jo, D. J. Kim, H. Sung, T. W. Noh, H. N. Lee, J. G. Yoon, and T. K. Song, "Domain Wall Motion in Epitaxial $Pb(Zr,Ti)O_3$ Capacitors Investigated by Modified Piezoresponse Force Microscopy," *Appl. Phys. Lett.*, **92** [25] 252901 (2008).

[83]P. Maksymovych, S. Jesse, M. Huijben, R. Ramesh, A. Morozovska, S. Choudhury, L. Q. Chen, A. P. Baddorf, and S. V. Kalinin, "Intrinsic Nucleation Mechanism and Disorder Effects in Polarization Switching on Ferroelectric Surfaces," *Phys. Rev. Lett.*, **102** [1] 017601 (2009).

[84]B. J. Rodriguez, S. Jesse, A. N. Morozovska, S. V. Svechnikov, D. A. Kiselev, A. L. Kholkin, A. A. Bokov, Z. G. Ye, and S. V. Kalinin, "Real Space Mapping of Polarization Dynamics and Hysteresis Loop Formation in Relaxor-Ferroelectric PbMg(1/3)Nb(2/3)O(3)-PbTiO(3) Solid Solutions," *J. Appl. Phys.*, **108** [4] 042006 (2010).

[85]A. Kumar, O. S. Ovchinnikov, H. Funakubo, S. Jesse, and S. V. Kalinin, "Real-Space Mapping of Dynamic Phenomena During Hysteresis Loop Measurements: Dynamic Switching Spectroscopy Piezoresponse Force Microscopy," *Appl. Phys. Lett.*, **98** [20] (2011).

[86]A. Gruverman, H. Tokumoto, A. S. Prakash, S. Aggarwal, B. Yang, M. Wuttig, R. Ramesh, O. Auciello, and T. Venkatesan, "Nanoscale Imaging of Domain Dynamics and Retention in Ferroelectric Thin Films," *Appl. Phys. Lett.*, **71** [24] 3492–4 (1997).

[87]S. Igor, C. Enrico, T. Alexander, S. S. N. Bharadwaja, H. Seungbum, S. Nava, S. C. Jeffrey, and T. Mineharu, "Unusual Size Effect on the Polarization Patterns in Micron-Size $Pb(Zr,Ti)O_3$ Film Capacitors," *Appl. Phys. Lett.*, **80** [25] 4804–6 (2002).

[88]P. Paruch, T. Giamarchi, and J. M. Triscone, "Domain Wall Creep in Mixed c-a Axis $Pb(Zr_{0.2}Ti_{0.8})O_3$ Thin Films," *Annalen Der Physik*, **13** [1–2] 95–6 (2004).

[89]F. Zavaliche, P. Shafer, R. Ramesh, M. P. Cruz, R. R. Das, D. M. Kim, and C. B. Eom, "Polarization Switching in Epitaxial $BiFeO_3$ Films," *Appl. Phys. Lett.*, **87** [25] 252902 (2005).

[90]P. Paruch and J. M. Triscone, "High-Temperature Ferroelectric Domain Stability in Epitaxial $PbZr_{0.2}Ti_{0.8}O_3$ Thin Films," *Appl. Phys. Lett.*, **88** [16] 162907 (2006).

[91]P. Shafer, F. Zavaliche, Y. H. Chu, P. L. Yang, M. P. Cruz, and R. Ramesh, "Planar Electrode Piezoelectric Force Microscopy to Study Electric Polarization Switching in $BiFeO_3$," *Appl. Phys. Lett.*, **90** [20] 202909 (2007).

[92]J. Y. Jo, S. M. Yang, T. H. Kim, H. N. Lee, J. G. Yoon, S. Park, Y. Jo, M. H. Jung, and T. W. Noh, "Nonlinear Dynamics of Domain-Wall Propagation in Epitaxial Ferroelectric Thin Films," *Phys. Rev. Lett.*, **102** [4] 045701 (2009).

[93]T. H. Kim, S. H. Baek, S. M. Yang, S. Y. Jang, D. Ortiz, T. K. Song, J. S. Chung, C. B. Eom, T. W. Noh, and J. G. Yoon, "Electric-Field-Controlled Directional Motion of Ferroelectric Domain Walls in Multiferroic $BiFeO_3$ Films," *Appl. Phys. Lett.*, **95** [26] 262902 (2009).

[94]V. Anbusathaiah, S. Jesse, M. A. Arredondo, F. C. Kartawidjaja, O. S. Ovchinnikov, J. Wang, S. V. Kalinin, and V. Nagarajan, "Ferroelastic Domain Wall Dynamics in Ferroelectric Bilayers," *Acta Mater.*, **58** [16] 5316–25 (2010).

[95]D. Wu, I. Vrejoiu, M. Alexe, and A. Gruverman, "Anisotropy of Domain Growth in Epitaxial Ferroelectric Capacitors," *Appl. Phys. Lett.*, **96** [11] 112903 (2010).

[96]J. Y. Jo, D. J. Kim, Y. S. Kim, S. B. Choe, T. K. Song, J. G. Yoon, and T. W. Noh, "Polarization Switching Dynamics Governed by the Thermodynamic Nucleation Process in Ultrathin Ferroelectric Films," *Phys. Rev. Lett.*, **97** [24] 247602 (2006).

[97]A. N. Morozovska, E. A. Eliseev, and S. V. Kalinin, "Domain Nucleation and Hysteresis Loop Shape in Piezoresponse Force Spectroscopy," *Appl. Phys. Lett.*, **89** [19] 192901 (2006).

[98]N. A. Polomoff, R. N. Premnath, J. L. Bosse, and B. D. Huey, "Ferroelectric Domain Switching Dynamics with Combined 20 nm and 10 ns Resolution," *J. Mater. Sci.*, **44** [19] 5189–96 (2009).

[99]Y. C. Chen, G. F. Wang, H. H. Tai, J. W. Chen, Y. C. Huang, J. C. Yang, and Y. H. Chu, "Non-Volatile Domain Nucleation and Growth in Multiferroic $BiFeO_3$ Films," *Nanotechnology*, **22** [25] 254030 (2011).

[100]V. Nagarajan, S. Aggarwal, A. Gruverman, R. Ramesh, and R. Waser, "Nanoscale Polarization Relaxation in a Polycrystalline Ferroelectric Thin Film: Role of Local Environments," *Appl. Phys. Lett.*, **86** [26] 262910 (2005).

[101]Y. Kim, S. Hong, H. Park, S. H. Kim, D. K. Min, and K. No, "Grain/Domain Interaction Antd its Effect on bit Formation in Ferroelectric Films," *Integr. Ferroelectr.*, **78**, 255–60 (2006).

[102]R. Nath, R. E. Garcia, J. E. Blendell, and B. D. Huey, "Influence of Grain Boundaries and Texture on Ferroelectric Domain Hysteresis," *JOM*, **59** [1] 17–21 (2007).

[103]B. J. Rodriguez, S. Jesse, A. P. Baddorf, T. Zhao, Y. H. Chu, R. Ramesh, E. A. Eliseev, A. N. Morozovska, and S. V. Kalinin, "Spatially Resolved Mapping of Ferroelectric Switching Behavior in Self-Assembled Multiferroic Nanostructures: Strain, Size, and Interface Effects," *Nanotechnology*, **18**, 405701 (2007).

[104]S. Wicks, K. Seal, S. Jesse, V. Anbusathaiah, S. Leach, R. E. Garcia, S. V. Kalinin, and V. Nagarajan, "Collective Dynamics in Nanostructured Polycrystalline Ferroelectric Thin Films Using Local Time-Resolved Measurements and Switching Spectroscopy," *Acta Mater.*, **58** [1] 67–75 (2010).

[105]S. Hong, B. Ecabart, E. L. Colla, and N. Setter, "Three-Dimensional Ferroelectric Domain Imaging of Bulk Pb(Zr,Ti)O-3 by Atomic Force Microscopy," *Appl. Phys. Lett.*, **84** [13] 2382–4 (2004).

[106]R. Gysel, A. K. Tagantsev, I. Stolichnov, N. Setter, and M. Pavius, "Ferroelectric Film Switching Via Oblique Domain Growth Observed by Cross-Sectional Nanoscale Imaging," *Appl. Phys. Lett.*, **89** [8] 082906 (2006).

[107]J. Y. Jo, P. Chen, R. J. Sichel, S. H. Baek, R. T. Smith, N. Balke, S. V. Kalinin, M. V. Holt, J. Maser, K. Evans-Lutterodt, C. B. Eom, and P. G. Evans, "Structural Consequences of Ferroelectric Nanolithography," *Nano Lett.*, **11** [8] 3080–4 (2011).

[108]J. Y. Jo, P. Chen, R. J. Sichel, S. J. Callori, J. Sinsheimer, E. M. Dufresne, M. Dawber, and P. G. Evans, "Nanosecond Dynamics of Ferroelectric/Dielectric Superlattices," *Phys. Rev. Lett.*, **107** [5] 055501 (2011).

[109]C. T. Nelson, P. Gao, J. R. Jokisaari, C. Heikes, C. Adamo, A. Melville, S. H. Baek, C. M. Folkman, B. Winchester, Y. J. Gu, Y. M. Liu, K. Zhang, E. G. Wang, J. Y. Li, L. Q. Chen, C. B. Eom, D. G. Schlom, and X. Q. Pan, "Domain Dynamics During Ferroelectric Switching," *Science*, **334** [6058] 968–71 (2011).

[110]A. Schilling, S. Prosandeev, R. G. P. McQuaid, L. Bellaiche, J. F. Scott, and J. M. Gregg, "Shape-Induced Phase Transition of Domain Patterns in Ferroelectric Platelets," *Phys. Rev. B*, **84** [6] 064110 (2011).

[111]R. B. Liu, R. Y. Guo, A. S. Bhalla, L. E. Cross, M. Levy, and R. M. Osgood, "Optical Observation of Dynamic Ferroelectric Phase Transition and Static Domain Structures in Crystal ion Sliced (CIS) $LiNbO_3$ Film," *Mater. Lett.*, **39** [5] 264–7 (1999).

[112]M. Paturzo, S. Grilli, P. Ferraro, A. Finizio, P. De Natale, N. Argiolas, M. Bazzan, M. V. Ciampolillo, and C. Sada, "Optical Characterization of Erbium Doped $LiNbO_3$ Poling Properties," *J. Appl. Phys.*, **104** [1] 014103 (2008).

[113]V. Y. Shur, E. V. Nikolaeva, E. I. Shishkin, V. L. Kozhevnikov, and A. P. Chernykh, "Kinetics of Domain Structure and Switching Currents in Single Crystals of Congruent and Stoichiometric Lithium Tantalate," *Phys. Solid State*, **44** [11] 2151–6 (2002).

[114]V. Gopalan, V. Dierolf, and D. A. Scrymgeour, "Defect-Domain Wall Interactions in Trigonal Ferroelectrics," *Annu. Rev. Mater. Res.*, **37**, 449–89 (2007).

[115]V. Dierolf, C. Sandmann, V. Gopalan, S. Kim, and K. Polgar, "Rearrangement of Rare Earth Defects Under Domain Inversion in LiNbO3," *Radiat. Eff. Defects Solids*, **158** [1–6] 247–50 (2003).

[116]V. Dierolf, C. Sandmann, S. Kim, V. Gopalan, and K. Polgar, "Ferroelectric Domain Imaging by Defect-Luminescence Microscopy," *J. Appl. Phys.*, **93** [4] 2295–7 (2003).

[117]S. Grilli, M. Paturzo, L. Miccio, and P. Ferraro, "*In Situ* Investigation of Periodic Poling in Congruent $LiNbO_3$ by Quantitative Interference Microscopy," *Meas. Sci. Technol.*, **19** [7] 074008 (2008).

[118]C. S. Ganpule, V. Nagarajan, H. Li, A. S. Ogale, D. E. Steinhauer, S. Aggarwal, E. Williams, R. Ramesh, and P. De Wolf, "Role of 90 Degrees Domains in Lead Zirconate Titanate Thin Films," *Appl. Phys. Lett.*, **77** [2] 292–4 (2000).

[119]B. D. Huey and R. Nath, "High-Speed Piezo Force Microscopy: Novel Observations of Ferroelectric Domain Poling, Nucleation, and Growth"; pp. 329–44 in *Scanning Probe Microscopy of Functional Materials*, Edited by S. V. Kalinin and A. Gruverman. Springer, New York, 2011.

[120]R. Landauer, "Electrostatic Considerations in $BaTiO_3$ Domain Formation During Polarization Reversal," *J. Appl. Phys.*, **28** [2] 227–34 (1957).

[121]A. N. Morozovska, E. A. Eliseev, Y. Li, S. V. Svechnikov, P. Maksymovych, V. Y. Shur, V. Gopalan, L.-Q. Chen, and S. V. Kalinin, "Thermo-

dynamics of Nanodomain Formation and Breakdown in Scanning Probe Microscopy: Landau-Ginzburg-Devonshire Approach," *Phys. Rev. B*, **80**, 214110 (2009).
[122]A. Grigoriev, D.-H. Do, D. M. Kim, C.-B. Eom, B. Adams, E. M. Dufresne, and P. G. Evans, "Nanosecond Domain Wall Dynamics in Ferroelectric $Pb(Zr,Ti)O_3$ Thin Films," *Phys. Rev. Lett.*, **96** [18] 187601–4 (2006).
[123]N. A. Polomoff and B. D. Huey, "Ferroelectric Domain Wall Velocities due to 10 nsec Electrical Pulsing." in. UConn IMS, 2008.
[124]Y. Ishibashi and Y. Takagi, "Note on Ferroelectric Domain Switching," *J. Phys. Soc. Jpn.*, **31**, 506–10 (1971).
[125]Y. Ishibashi, "Polarization Reversal Kinetics in Ferroelectric Liquid Crystals," *Jpn. J. Appl. Phys.*, **24**, 126–9 (1985).
[126]K. Dimmler, M. Parris, D. Butler, S. Eaton, B. Pouligny, J. F. Scott, and Y. Ishibashi, "Switching Kinetics in KNO_3 Ferroelectric Thin-Film Memories," *J. Appl. Phys.*, **61** [12] 5467–70 (1987).
[127]R. N. Premnath, *High Speed Piezo Force Microscopy*. in MS&E, Vol. PhD. University of Connecticut, Storrs, CT, 2009.
[128]A. Gruverman, D. Wu, and J. F. Scott, "Piezoresponse Force Microscopy Studies of Switching Behavior of Ferroelectric Capacitors on a 100-ns Time Scale," *Phys. Rev. Lett.*, **100** [9] 097601 (2008).
[129]S. V. Kalinin, B. J. Rodriguez, S. Jesse, Y. H. Chu, T. Zhao, R. Ramesh, S. Choudhury, L. Q. Chen, E. A. Eliseev, and A. N. Morozovska, "Intrinsic Single-Domain Switching in Ferroelectric Materials on a Nearly Ideal Surface," *Proc. Natl. Acad. Sci. USA*, **104** [51] 20204–9 (2007).
[130]P. Maksymovych, N. Balke, S. Jesse, M. Huijben, R. Ramesh, A. P. Baddorf, and S. V. Kalinin, "Defect-Induced Asymmetry of Local Hysteresis Loops on $BiFeO_3$ Surfaces," *J. Mater. Sci.*, **44** [19] 5095–101 (2009).
[131]B. J. Rodriguez, S. Choudhury, Y. H. Chu, A. Bhattacharyya, S. Jesse, K. Seal, A. P. Baddorf, R. Ramesh, L. Q. Chen, and S. V. Kalinin, "Unraveling Deterministic Mesoscopic Polarization Switching Mechanisms: Spatially Resolved Studies of a Tilt Grain Boundary in Bismuth Ferrite," *Adv. Funct. Mater.*, **19** [13] 2053–63 (2009).
[132]S. V. Kalinin, B. J. Rodriguez, A. Y. Borisevich, A. P. Baddorf, N. Balke, H. J. Chang, L. Q. Chen, S. Choudhury, S. Jesse, P. Maksymovych, M. P. Nikiforov, and S. J. Pennycook, "Defect-Mediated Polarization Switching in Ferroelectrics and Related Materials: From Mesoscopic Mechanisms to Atomistic Control," *Adv. Mater.*, **22** [3] 314–22 (2010).
[133]S. V. Kalinin, S. Jesse, A. Tselev, A. P. Baddorf, and N. Balke, "The Role of Electrochemical Phenomena in Scanning Probe Microscopy of Ferroelectric Thin Films," *Acs Nano*, **5** [7] 5683–91 (2011).
[134]F. Peter, J. Kubacki, K. Szot, B. Reichenberg, and R. Waser, "Influence of Adsorbates on the Piezoresponse of $KNbO_3$," *Phys. Status Solidi a Appl. Mater. Sci.*, **203** [3] 616–21 (2006).
[135]A. N. Morozovska, S. V. Svechnikov, E. A. Eliseev, B. J. Rodriguez, S. Jesse, and S. V. Kalinin, "Local Polarization Switching in the Presence of Surface-Charged Defects: Microscopic Mechanisms and Piezoresponse Force Spectroscopy Observations," *Phys. Rev. B*, **78** [5] 054101 (2008).
[136]J. W. V. Cahn, "The Time Cone Method for Nucleation and Growth Kinetics on a Finite Domain"; pp. 425–38 in *Thermodynamics and Kinetics of Phase Transformations*. Vol. 398, Edited by J. H. Perepezko and D. R. Allen. M. R. Society, Boston, MA, 1996.
[137]A. N. Komogorov, "Statistical Theory of Metal Crystallization," *Izv. Akad. Nauk SSSR*, **1**, 355–9 (1937).
[138]M. Avrami, "Kinetics of Phase Change-I," *J. Chem. Phys.*, **7** [12] 1103–12 (1939).
[139]W. A. Johnson and R. F. Mehl, "Reaction Kinetics in Processes of Nucleation and Growth," *Trans. AIME*, **135**, 416–42 (1939).
[140]M. Avrami, "Kinetics of Phase Change-II. Transformation-Time Relations for Random Distribution of Nuclei," *J. Chem. Phys.*, **8** [2] 212–24 (1940).
[141]M. Avrami, "Kinetics of Phase Change-III. Granulation, Phase Change, and Microstructure," *J. Chem. Phys.*, **9** [2] 177–84 (1941).
[142]H. Orihara, S. Hashimoto, and Y. Ishibashi, "A Theory of D-E Hysteresis Loop Based on the Avrami Model," *J. Phys. Soc. Jpn.*, **63**, 1031–5 (1994).
[143]R. W. Balluffi, S. M. Allen, and W. C. Carter, *Kinetics of Materials*. John Wiley and Sons, Hoboken, NJ, 2005.
[144]D. Hesse and M. Alexe, "Interfaces in Nanosize Perovskite Titanate Ferroelectrics – Microstructure and Impact on Selected Properties," *Zeitschrift Fur Metallkunde*, **96** [5] 448–51 (2005).
[145]Y. Ivry, D. P. Chu, J. F. Scott, and C. Durkan, "Domains Beyond the Grain Boundary," *Adv. Funct. Mater.*, **21** [10] 1827–32 (2011).
[146]X. Leng, H. R. Zeng, X. M. Li, Y. He, K. Y. Zhao, and W. Wang, "Unusual Piezoresponse Behavior Across the Grain Boundary of PbMg(1/3)Nb(2/3)O(3)-0.33PbTiO(3) Thin Films," *Appl. Surf. Sci.*, **257** [18] 8085–8 (2011).
[147]J. F. Scott, A. Gruverman, D. Wu, I. Vrejoiu, and M. Alexe, "Nanodomain Faceting in Ferroelectrics," *J. Phys. Condes. Matter*, **20** [42] 425222 (2008).
[148]Y. Kim, Y. Cho, S. Hong, S. Buhlmann, H. Park, D. K. Min, S. H. Kim, and K. No, "Correlation Between Grain Size and Domain Size Distributions in Ferroelectric Media for Probe Storage Applications," *Appl. Phys. Lett.*, **89** [16] 162907 (2006).
[149]S. V. Kalinin, R. Shao, and D. A. Bonnell, "Local Phenomena in Oxides by Advanced Scanning Probe Microscopy," *J. Am. Ceram. Soc.*, **88** [5] 1077–98 (2005).
[150]R. E. Garcia, B. D. Huey, and J. E. Blendell, "Virtual Piezoforce Microscopy of Polycrystalline Ferroelectric Films," *J. Appl. Phys.*, **100** [6] 064105 (2006).
[151]B. J. Rodriguez, Y. H. Chu, R. Ramesh, and S. V. Kalinin, "Ferroelectric Domain Wall Pinning at a Bicrystal Grain Boundary in Bismuth Ferrite," *Appl. Phys. Lett.*, **93** [14] 142901 (2008).
[152]Y. Kim, Y. Cho, S. Hong, S. Buhlmann, H. Park, D. K. Min, S. H. Kim, and K. No, "Tip Traveling and Grain Boundary Effects in Domain Formation Using Piezoelectric Force Microscopy for Probe Storage Applications," *Appl. Phys. Lett.*, **89** [17] 172909 (2006).
[153]A. Gruverman, B. J. Rodriguez, A. I. Kingon, R. J. Nemanich, A. K. Tagantsev, J. S. Cross, and M. Tsukada, "Mechanical Stress Effect on Imprint Behavior of Integrated Ferroelectric Capacitors," *Appl. Phys. Lett.*, **83** [4] 728 (2003).
[154]M. Dawber, N. Stucki, C. Lichtensteiger, S. Gariglio, P. Ghosez, and J.-M. Triscone, "Tailoring the Properties of Artificially Layered Ferroelectric Superlattices," *Adv. Mater.*, **19** [23] 4153–9 (2007).
[155]M. Dawber, N. Stucki, C. Lichtensteiger, S. Gariglio, and J.-M. Triscone, "New Phenomena at the Interfaces of Very Thin Ferroelectric Oxides," *J. Phys. Condens. Matter*, **20** [26] 264015 (2008).
[156]D. G. Schlom, L.-Q. Chen, X. Pan, A. Schmehl, and M. A. Zurbuchen, "A Thin Film Approach to Engineering Functionality into Oxides," *J. Am. Ceram. Soc.*, **91** [8] 2429–54 (2008).
[157]X. Tan and J. K. Shang, "Intersection of a Domains in the c-Domain Matrix Driven by Electric Field in Tetragonal Ferroelectric Crystal," *J. Appl. Phys.*, **96** [5] 2805–10 (2004).
[158]F.-X. Li, S. Li, and D.-N. Fang, "Domain Switching in Ferroelectric Single Crystal/Ceramics Under Electromechanical Loading," *Mater. Sci. Eng. B*, **120** [1–3] 119–24 (2005).
[159]J. Desmarais, J. F. Ihlefeld, T. Heeg, J. Schubert, D. G. Schlom, and B. D. Huey, "Mapping and Statistics of Ferroelectric Domain Boundary Angles and Types," *Appl. Phys. Lett.*, **99**, 162902 (2011).
[160]N. A. Polomoff, S. Lee, and B. D. Huey, "Strategy for Low Power, High Speed Ferroelectric Switching," to be submitted (2011). □

Bryan Douglas Huey, PhD, is an Associate Professor at the University of Connecticut in the department of Chemical, Materials, and Biomolecular Engineering. He also holds a Velux visiting professorship to Aarhus University's Interdisciplinary Nanoscience Center, iNANO. Huey's "nmLabs" at UConn's Institute of Materials Science specialize in the development and application of Scanning Probe Microscopy, with recent thrusts in high speed scanning as well as AFM coupled with 3-d optics. Materials systems of particular interest include ferroelectric and phase change thin films, fuel cells, blast-resistant materials, nano-formulated pharmaceuticals, living biological cells, biomolecules, and cell scaffold materials. Huey is the current program co-chair for the ACerS Basic Science Division.

Ramesh Nath Premnath, PhD, is currently a Publishing Editor with the Applied Science Department, Springer Science and Business Media, Singapore. Prior to this, he was a researcher at the Institute of Materials Research and Engineering, Singapore (2010-2011), and a post-doctoral researcher at Argonne National Laboratory, USA (2008-2010). For his PhD work at the University of Connecticut with B. D. Huey, Ramesh was awarded a sapphire medal in the ACerS Graduate Excellence in Materials Science competition, 2007. His research interests include piezoelectric, ferroelectric, and multiferroic oxide structures for non-volatile memory and energy harvesting applications; scanning probe microscopy to study domains, switching, and polarization dynamics in ferroic thin films; and scaling studies using electric and magnetic force microscopy. Dr. Premnath has been a member of ACerS since 2007.

Sungjun Lee, PhD, has been a principal researcher at the Korea Research Institute of Standards and Science (KIRSS) since 2005. Sungjun was in B. D. Huey's research labs as a guest researcher in 2009-2010. Dr. Lee's interests and expertise include Scanning Tunneling Microscopy in ultra-high vacuum, carbon nanotubes, semiconductor transport measurements, nanomechanics, nanoscale mass standards, and high speed SPM implementation.

Nicholas Alexander Polomoff, PhD, MBA, MS, is currently a senior materials scientist at Material ConneXion in New York City, researching and promoting novel materials for design purposes. In 2011 Nick earned a PhD with B. D. Huey at UConn, "HS-SPM Mapping of Ferroelectric Domain Dynamics with Combined Nanoscale and Nanosecond Resolution," following a MS in 2008. Nick has a BS in Ceramics and Materials Science from Clemson University, as well as a business administration minor, both in 2004. In 2010, Dr. Polomoff also earned an MBA from UConn in Finance and Marketing.